Title: A novel method for reliably measuring miniature and spontaneous postsynaptic potentials/currents in whole-cell patch clamp recordings in the central nervous system

Author Names and Affiliations: Martynas Dervinis[1], Guy Major[1]

[1]: School of Biosciences, Cardiff University, Cardiff, Wales, CF10 3AT, UK

Corresponding author email address: martynas.dervinis@gmail.com

Number of pages: 61

Number of figures: 13

Abstract: 232

Body text excluding Materials and Methods: 5896

Conflict of interest statement: The authors declare no competing financial interests.

Acknowledgements: Cardiff University (GM, MD), The Medical Research Council of the UK (MD PhD)

Abstract

Measurements of miniature postsynaptic currents (mPSCs) or potentials (mPSPs) in the soma of neurons of the central nervous system (CNS) provide a way of quantifying the synaptic function at the network level and, therefore, are routine in the neurophysiology literature. These miniature responses (or 'minis') are thought to be elicited by the spontaneous release of a single neurotransmitter vesicle, also called quantum. As such their measurement at the soma can potentially offer a technically straightforward way of estimating 'quantal sizes' of central synapses. However, popular methods for detecting minis in whole-cell recordings fall short of being able to reliably distinguish them from background physiological noise. This issue has received very limited attention in the literature and its scope as well as the relative performance of existing algorithms have not been quantified. As a result, solutions for reliably measuring the quantal size in somatic recordings also do not exist. As the first step in proposing and testing a potential solution, we developed and described a novel mPSP/mPSC detection algorithm as part of our quantal analysis software called 'minis'. We tested its performance in detecting real and simulated minis in whole-cell recordings from pyramidal neurons in rat neocortical slices and compared it to two of the most-used mini detection algorithms. This benchmarking revealed superior detection by our algorithm. The release version of the algorithm also offers great flexibility via graphical and programming interfaces.

42 # Abbreviations

43 ABF – Axon Binary File

44 aCSF – artificial cerebrospinal fluid

45 AMPA – α-amino-3-hydroxy-5-methyl-4-isoxazolepropionic acid

46 AP – action potential

47 API - application programming interface

48 AUC – area under the curve

49 CNS – central nervous system

50 CPP – (*RS*)-3-(2-carboxypiperazin-4-yl)-propyl-1-phosphonic acid

51 d' – sensitivity index 'd-prime' (defined in Methods)

52 EPSC – excitatory postsynaptic current

53 EPSP – excitatory postsynaptic potential

54 FNR – false negative rate ('miss' rate)

55 FPR – false positive rate ('false alarm' rate)

56 GABA – gamma-aminobutyric acid

57 IPSC – inhibitory post-synaptic current

58 IPSP – inhibitory post-synaptic potential

59 mEPSC– miniature excitatory post-synaptic current

60 mEPSP– miniature excitatory post-synaptic potential

61 mIPSC– miniature inhibitory post-synaptic current

62 mIPSP– miniature inhibitory post-synaptic potential

63 mPSC – miniature post-synaptic current

64 mPSP – miniature post-synaptic potential

65 NBQX – 2,3-dioxo-6-nitro-1,2,3,4-tetrahydrobenzo[*f*]quinoxaline-7-sulfonamide

66 NMDA – N-methyl-D-aspartate

67 ROC – receiver operator characteristic

68 sEPSC– spontaneous excitatory post-synaptic current

69 sEPSP– spontaneous excitatory post-synaptic potential

70 sIPSC– spontaneous inhibitory post-synaptic current

71 sIPSP– spontaneous inhibitory post-synaptic potential

72 smEPSC – simulated mEPSC

73 smEPSP – simulated mEPSP

74 smPSC – simulated mPSC

75 smPSP – simulated mPSP

76 sPSC – spontaneous post-synaptic current

77 sPSP – spontaneous post-synaptic potential

78 TNR – true negative rate

79 TPR – true positive rate ('hit' rate, sensitivity)

80 TTX – tetrodotoxin

81 V_m – membrane potential

v-ROC – virtual ROC (ROC-like plot)

Introduction

Miniature postsynaptic potentials (mPSPs; under voltage recording) or currents (mPSCs; under voltage clamp), often simply called minis, are thought to correspond to the postsynaptic response to a spontaneous release of a single neurotransmitter vesicle (Brown et al., 1979; del Castillo and Katz, 1954; Fatt and Katz, 1952; Isaacson and Walmsley, 1995; Wall and Usowicz, 1998). Somatic measurements of their properties in the CNS provide a window onto the synaptic function at the network level and, therefore, are routine in the literature. Their kinetics (i.e., rise and decay times) are thought to reflect the underlying kinetics of individual ion channels (α-amino-3-hydroxy-5-methyl-4-isoxazolepropionic acid receptors, AMPARs (Sara et al., 2011), or γ-Aminobutyric acid type A receptors, $GABA_A$Rs (El Khoueiry et al., 2022); i.e., their probabilities of opening and staying open) (De Koninck and Mody, 1994), as well as the locations of the source synapses across the neuronal dendritic tree (proximal vs. distal) and the passive electric properties of neuronal membranes (Agmon-Snir and Segev, 1993; Major et al., 1994; Rinzel and Rall, 1974). Their incidence rates (often called frequencies, although they do not occur rhythmically) are typically thought to reflect the overall number of active synapses on the dendritic tree (Isaac et al., 1995; Liao et al., 1995; Segal, 2010) but can also be indicative of the rate at which presynaptic vesicles are fusing spontaneously with the neuronal membrane (Glasgow et al., 2019). Finally, the size of the mean amplitude of minis is often thought to reflect the overall strength of synapses across the dendritic tree (Segal, 2010). Assuming that minis are postsynaptic responses to the release of a single neurotransmitter vesicle, their amplitude measurements at the soma can also be used as a straightforward method of estimating the quantal size of synapses onto a recorded neuron. These estimates should, however, be viewed with caution as minis amplitudes at the soma tend to be small and difficult to distinguish from noise in the CNS (Larkum et al., 2009; Major et al., 2013; Nevian et al., 2007; Stuart and Spruston, 1998; Williams and Mitchell, 2008; Williams and Stuart, 2002).

‘Template matching’ and ‘thresholded amplitude detection’ have emerged as the two main approaches to detecting minis (Shi et al., 2010). The first approach relies on the observation that minis often have a fast rise phase and a slower decay phase while noise fluctuation typically do not show such regularities (Liao et al., 1992; Rall, 1967). The somatic current or voltage recording trace is scanned with a sliding window and an average minis template is scaled and fitted to the traces to detect minis-like events of varying amplitudes (Clements and Bekkers, 1997). This approach has been implemented in a commercially available software suite pClamp (Clampfit application). The second approach detects peaks in the recording traces and applies an amplitude threshold combined with shape criteria like the fast rise time and often a limit on the area under the trace (total charge) (Clements and Bekkers, 1997; Shi et al., 2010). This approach has been implemented in a popular commercially available software application MiniAnalysis.

‘Thresholded amplitude detection’ algorithms are thought to suffer from a lack in selectivity (Clements and Bekkers, 1997). As a result, their performance can either inflate false positive detection rates and confuse noise fluctuations with the small amplitude minis if a low amplitude threshold is used or inflate false negative rejection rates and bias the detection towards large amplitude events if a large amplitude detection threshold is used instead. Similarly, change in the signal to noise ratio due to changes in the noise level or the amplitude of minis would artifactually affect estimates of both amplitudes and incidence rates of minis. ‘Template matching’ algorithms were introduced as a remedy to the selectivity problem (Clements and Bekkers, 1997), yet in practice they were found to bias detection towards unambiguous clearcut PSPs that often were also large, and, therefore, they suffer from the opposite problem of the lack in sensitivity (Hwang and Copenhagen, 1999). The lower popularity of ‘template matching’ algorithms compared to their counterpart suggests this problem to be more severe than the one intended to be remedied.

Given these considerations and our goal of developing a reliable method for estimating quantal sizes of central synapses based on minis' amplitude somatic measurements (presented in the companion article), we developed a novel algorithm, called 'minis', to detect miniature (and action potential (AP)-triggered) postsynaptic events. A novel algorithm was needed for several reasons. Firstly, existing algorithms have not been described in sufficient detail in the peer-reviewed literature. Popular algorithms like MiniAnalysis and Clampfit are proprietary. Secondly, because existing algorithms are not open, they are not modifiable. Thus, they cannot be automated and integrated with other software. Lastly, existing algorithms have not yet, to our knowledge, been benchmarked in peer-reviewed articles. To fill these gaps, we developed an algorithm that is transparent, flexible, open-source, and objectively evaluated using standardised criteria.

Materials and Methods

Published values for amplitudes and incidence rates of minis.

We searched the neuroscience literature between January 1, 2020 – January 31, 2022 for a representative sample of recently reported amplitudes and incidence rate of miniature excitatory postsynaptic currents (mEPSCs) and potentials (mEPSPs) in cortical pyramidal cells, and common data analysis practices in the CNS. We also compared reported mEPSC rates per second to a predicted range of values. We limited our search to publications in English only that reported research results on synaptic function in the CNS. We examined the title and abstract fields of studies in MEDLINE database using the PubMed search engine with the following search keywords: ("spontaneous neurotransmission" OR "spontaneous neurotransmitter release" OR "spontaneous transmitter release" OR "spontaneous postsynaptic" OR "miniature postsynaptic" OR "mEPSP" OR "mEPSC" OR "mPSP" OR "mPSC" OR "mIPSP" OR "mIPSC" OR OR "sEPSP"[Title/Abstract] OR "sEPSC"[Title/Abstract] OR "sPSP"[Title/Abstract] OR "sPSC"[Title/Abstract] OR "sIPSP"[Title/Abstract] OR "sIPSC"[Title/Abstract]) AND ("cortex"[Title/Abstract] OR "cortical"[Title/Abstract] OR "neocortex"[Title/Abstract] OR "neocortical"[Title/Abstract] OR "hippocampus"[Title/Abstract] OR "hippocampal"[Title/Abstract] OR "thalamus"[Title/Abstract] OR "thalamic"[Title/Abstract] OR "brain"[Title/Abstract] OR "cerebral"[Title/Abstract] OR "central nervous system"[Title/Abstract] OR "pyramidal"[Title/Abstract] OR "CNS"[Title/Abstract]). Abbreviations ending in PSP and PP stand for postsynaptic potentials, while PSC and PC stand for postsynaptic currents and should not be confused with end-plate potentials and currents.

Animals and electrophysiology

All experimental procedures were carried out in accordance with the UK Animals (Scientific Procedures) Act 1986 at Cardiff University under Home Office personal and project licenses.

169 19 to 27-day old Wistar rats (RRID:RGD_13508588; n = 11) of either sex were anaesthetised with
170 isoflurane and decapitated, and the brain removed under cold (0-2 °C) artificial cerebrospinal fluid
171 (aCSF), composed of (in mM) 125 NaCl, 26 $NaHCO_3$, 2.3 KCl, 1.26 KH_2PO_4, 1 $MgSO_4$, 10 glucose, and 2
172 $CaCl_2$ bubbled with 95% O_2 5%CO_2. Coronal somatosensory cortical slices 350 µm thick were cut and
173 held in an interface chamber with their surfaces kept moist for 1 to 3 hours by aCSF at room
174 temperature (21-23°C) under a 95% O_2 5% CO_2 atmosphere. Individual slices were then placed in the
175 recording chamber and held at 35-37°C with aCSF flowing over both surfaces. For recording
176 purposes at 35-37°C the aCSF solution contained (in mM) 125 NaCl, 24 $NaHCO_3$, 2.3 KCl, 1.26 KH_2PO_4,
177 1 $MgSO_4$, 10 glucose, and 2 $CaCl_2$.
178
179 Whole-cell recordings (n = 14) were obtained under visual control using infrared scanning gradient
180 contrast imaging with the imaging laser beam and a Dodt tube. Recordings were made with 4.5-9
181 MΩ borosilicate glass pipettes (Harvard Apparatus, 1.5 mm outside diameter and 0.86 mm, internal
182 diameter, omega-dot filament; Sutter P2000 puller), filled with (mM): 140 KGluconate, 10 HEPES, 2
183 $MgCl_2$, 3 ATP-Na_2, 0.3 GTP-Na, 0.1 Magnesium Green, 0.1 Alexa 594; 7.35 pH, 273 mOsm/L
184 osmolarity. Signals were amplified, low-pass filtered (5 KHz) and digitised (Axopatch-200B, custom
185 amplifier/filters, Digidata 1440, Clampex software; Molecular Devices). Pipettes and electrodes were
186 positioned with Sutter MP265 and 285 manipulators with a diagonal (axial) mode, using
187 parallelogram trajectories.
188
189 The electrophysiological recordings consisted of two phases. During the first phase we recorded
190 mEPSPs against the background of physiological noise ('noise + minis' condition) by applying aCSF
191 with AP and inhibitory postsynaptic potential blockers added: 0.5 or 1 µM tetrodotoxin (TTX;
192 selective, potent Na^+ channel blocker), and 12.5 µM gabazine (selective, potent $GABA_A$ receptor
193 antagonist to block (fast components) of inhibitory synaptic inputs – IPSCs and resulting IPSPs). AP
194 blockade by TTX was explicitly tested for with long current pulses pushing membrane potential (V_m)

195 well above normal AP threshold levels, to around -20 mV. The average duration of this phase of the
196 recordings was 21.8 (± s.d. 0.9) minutes. During a second phase, we recorded noise with mEPSPs
197 blocked ('noise-alone' condition). This recording was carried out after further adding 40 µM 2,3-
198 dioxo-6-nitro-7-sulfamoyl-benzo[f]quinoxaline (NBQX) (selective, potent α-amino-3-hydroxy-5-
199 methyl-4-isoxazolepropionic acid (AMPA) receptor antagonist) and 50 µM CPP (competitive, non-use
200 dependent selective N-methyl-D-aspartate (NMDA) receptor antagonist) to the solution used in the
201 'noise + minis' condition, to block all excitatory glutamatergic synaptic inputs (and thus EPSPs),
202 verified by inspecting and analysing the traces across a number of recordings with the same flow
203 rates. The average duration of this phase of the recordings was 44.8 (± s.d. 2.9) minutes.
204
205 **Experimental design**
206 The goal of this benchmarking study was to compare mEPSP detection performance by three
207 different detection algorithms, mainly in terms of standard signal detection theory measures. Two of
208 them were the most popular software products used in the field of synaptic function research in the
209 CNS, while the third one was our novel algorithm called 'minis'.
210
211 Current clamp whole-cell patch recordings obtained during the initial recording phase ('noise +
212 minis' condition) underwent mEPSP detection analysis using 'minis', MiniAnalysis (Bluecell;
213 RRID:SCR_002184), and Clampfit (part of the pClamp software suite, Molecular Devices;
214 RRID:SCR_011323). Detected mEPSPs were analysed in terms of their amplitude, 10-90% rise and
215 decay times, and incidence rate.
216
217 The current clamp recordings obtained during the second recording phase ('noise-alone' condition)
218 served as the background data in the mEPSP ('simulated minis') computer simulations (n=14 cells).
219 Computationally simulated mEPSPs (smEPSPs) were added onto segments of these V_m noise
220 recordings (1 of them 200 seconds, 1 more of them 40 seconds, while the remaining 12 were 100

221 seconds long) and the resultant hybrid waveforms (noise + simulated minis) were then subjected to
222 mEPSP detection analyses using 'minis', MiniAnalysis, and Clampfit software. Detection performance
223 was quantified using signal detection theory measures and compared between the three algorithms.
224
225 **Simulations**
226 *Simulating distributions of miniature excitatory postsynaptic potentials with a range of amplitudes*
227 *and rise times*
228 All simulations were carried out within the 'minis' software environment which is based on Matlab
229 (Mathworks; RRID:SCR_001622). Simulation of minis-like events was based on an analytical solution
230 to the passive cable equation for a transient current (Rall, 1977) using 100 lumped terms with a
231 double exponential synaptic current with τ_1= 0.1 ms and τ_2 = 2 ms (Major et al., 1993).
232
233 For a given membrane time constant, an initial cable segment was constructed with an electrotonic
234 length l/λ = 0.6, where l is the physical length of a dendrite (µm) and λ is the length (µm) constant
235 (Rall, 1977). Charge (Q) was injected at a location (x µm) along this cable and the resulting simulated
236 postsynaptic V_m was measured at one end of this cable segment. The precise location of the injected
237 charge was varied systematically, depending on the desired shape of the simulated event. Increasing
238 the distance of the injected charge along the cable away from the measurement site gradually
239 increased the rise time of the simulated event. To further increase the rise time, electrotonic length
240 was gradually increased until the required rise time was obtained. Increasing the amount of injected
241 charge increased the amplitude of the simulated event. Therefore, one was able to construct a
242 simulated postsynaptic potential of any rise time or amplitude, for the particular membrane time
243 constant used. A pool of simulated events could be created having any kind of distribution of
244 amplitudes and rise times, for a given decay time constant, with individual events' onsets
245 timed/placed pseudo-randomly along the time axis of the V_m recording.
246

Simulations used to construct full receiver operating characteristic (ROC)-like curves, using relatively fixed but realistic ('moderately-sized') mini amplitudes

All simulated mEPSPs were drawn from a two-dimensional normal distribution (independent amplitude and rise time dimensions) with the following amplitude parameters: mean μ_1 = 0.3 mV and standard deviation σ_1 = 0.05 mV (i.e., amplitudes relatively constant, with a relatively small amount of variation). The following (independent) 10-90% rise time parameters were used: μ_2 = 0.05 ms and σ_2 = 2.5 ms (with a minimum rise time of 0.05 ms; i.e., only upper half of normal distribution used). Simulated events were drawn pseudo-randomly from a distribution at one of the following incidence rates (minis/second): 640, 320, 160, 80, 40, 20, 10, 5, 2.5, 2.5, 2.5, 2.5, 2.5, and 2.5. Corresponding noise amplitude scale factors for these 14 incidence rates conditions were as follows: 1, 1, 1, 1, 1, 1, 1, 1, 1, 1.2, 1.4, 1.8, 2.6, and 4.2. The simulated events were then positioned at pseudo-randomly determined times along the V_m noise recording epochs obtained during the second recording phase ('noise-alone' condition). Two of the noise-alone epochs were 200 and 40 seconds long, while the remaining twelve were 100 seconds long. Four different simulation traces per recording, each of them having different pseudo-random event timings, were generated for every incidence rate/noise scale condition, resulting in a total number of 14×4×14 = 784 traces.

Simulations of miniature excitatory postsynaptic potentials using a range of biologically realistic amplitudes at realistic incidence rates

The simulation parameters used to construct full ROC-like curves cover only a part of the likely biological range. In reality, in cortex, minis vary far more in their amplitudes, with large numbers of smaller minis, but a minority of bigger minis too - some much bigger. Therefore, we set out to compare all three algorithms using a range of plausible simulated mini amplitudes, within the restricted range of what we deemed to be realistic incidence rates based on our estimation (from recent peer-reviewed publications) in the first Results subsection.

273 All simulated events were drawn from a two-dimensional distribution with the following
274 parameters: amplitudes were chosen from ten discrete values (0.05, 0.1, 0.15, 0.2, 0.25, 0.3, 0.35,
275 0.4, 0.45, 0.5 mV) with equal probabilities, rise times were independently chosen from the upper
276 half of a normal distribution with mean μ_2 = 0.05 ms, and standard deviation σ_2 = 2.5 ms (i.e., no rise
277 time shorter than 0.05 ms). Three 'realistic' minis' incidence rates were used: either 61, 38, or 27
278 minis/s. The simulated events were positioned at pseudo-random times along the same noise
279 recording epochs as used in the previous subsection. Four different simulation traces per recording,
280 each of them with different random event timings, were generated for every incidence rate
281 condition, resulting in a total number of 3×4×14 = 168 traces.
282
283 **Detection of spontaneous and miniature postsynaptic potentials**
284 *'minis' detection algorithm*
285 We developed a new algorithm to detect postsynaptic potentials and currents, that we have
286 incorporated into a data analysis software package called 'minis', coded in Matlab (Mathworks). It is
287 distributed as an application programming interface (API) in the form of a packaged Matlab app or a
288 Python (Python Software Foundation; RRID:SCR_008394) package or as a compiled standalone
289 desktop application with a graphical user interface. In brief, the detection algorithm takes a filtered
290 V_m or clamp current trace in the Axon Binary File (ABF) format and detects peaks and rising phases
291 and estimates their amplitudes and rise and decay times after applying certain processing steps.
292 These steps are outlined below (with parameter values tailored for detecting smEPSPs in cortical
293 pyramidal neurons). A schematic illustration of the key steps is shown in Figure 1:
294 A. Steps to find minis:
295 1. The data can be band-stop filtered to remove mains noise (e.g., small integer multiples of
296 50 Hz frequency components: optional). For this, a Butterworth filter (Matlab's 'butter'
297 function) is used with a stopband attenuation of 10 dB and a passband 'ripple' of 0.05 dB.
298 The stopband size is 1 Hz, and the passband is the entire remaining frequency range except

for the ±3 Hz window either side of the stopband frequency. Filtering effects are illustrated in Figure 2.

2. The recording trace can be smoothed using a Gaussian window (optional). We use a 1.5-millisecond window (with standard deviation of the Gaussian of 0.53 ms). This step removes high frequency noise. Smoothing effects are illustrated in Figure 2.
3. Peaks (local maxima) are identified in the filtered, smoothed recording trace. Each peak is then examined consecutively, starting with the initial peak.
4. Going through all the peaks one by one, any peak within the "Peak Integration Period" ('duration') following the current ('working') peak of interest is discarded if it is *smaller* (lower) than the peak of interest. For the analysis in this paper, we use a Peak Integration Period of 2.5 ms; this can be matched to the different 'sharpnesses' or 'breadths' of peaks in different data.
5. If there is a larger peak within the peak integration period, the 'working' peak of interest is moved to this new peak, and the old peak and all intervening peaks between it and the new 'working' peak of interest are discarded.
6. The baseline of the peak is positioned asymmetrically around the lowest value (local minimum) before the peak. Because of the faster upstroke of minis, compared with their decays, 80% of the baseline period falls before the lowest voltage (local minimum) and the remaining 20% after it (see Figure 1, inset). The interval from the baseline to the peak is limited by the *Maximum Time-to-Peak* parameter (10 ms used here). The last 20% of the baseline cannot start earlier than this.
7. The length in time of the baseline is controlled by the *baseline duration* parameter. We used 2-ms. (N.B. a baseline, or indeed an entire mini, can occur during the summated decay 'tails' of previous minis, particularly when the minis incidence rate is high relative to their decay time, as often seen with mPSPs under voltage recording at body temperature – but also under voltage clamp).

8. If the baseline overlaps with or falls before the previous peak, its start is delayed till immediately after the previous peak (to stop the baseline being pulled down by the previous rising phase), but the end time is kept the same.
9. To reject any large artefactual 'glitches', or small events that are putative noise, if the amplitude of the peak is outside of the range of acceptable amplitudes, between a detection threshold and a maximum, the peak is discarded. We allowed a range of amplitudes of 0.1-10 mV in detection conditions used to construct full 'virtual' receiver operating characteristic (ROC) curves. In other conditions we applied a range of 0.05-10 mV. To detect real minis, we used a range of 0.01-10 mV. (N.B. 0.02 or 0.03 mV detection thresholds can also be used for real whole-cell patch recording data from neocortical pyramidal neurons, under our experimental conditions, guided by the range of amplitudes of dendritically detected, somatically recorded mEPSPs in (Nevian et al., 2007) from layer 5 pyramidal neurons from rat somatosensory cortex; in general, detection thresholds will need to be adjusted to the cell type and experimental conditions).

B. Steps against multiple small minis being erroneously lumped together (merged):

10. Rising phase asymmetries: if the first half of the rise time (10-50% or 20-50%, depending on the rise time duration of choice) is longer than the second half (50-90% or 50-80%) by a factor of 5 or more (an asymmetry incompatible with typical single, non-summating EPSP or EPSC rising phases), the end of the baseline is extended slightly into the 'take-off' of the rising phase. (This correction can be repeated one more time).
11. The amplitude range test is applied again (Step 9).
12. If the second half of the rise time is longer than the first half by a factor of 5 or more, the peak is shifted to a previously discarded smaller peak, if exists. (Two minis could be summating on their rising phases, which is treated as a single mini, or the second mini could occur just after the peak of the first, which is treated as two minis, if two peaks are distinguishable).

13. The amplitude range test is applied again (Step 9).
14. If the 10% or 20% rise time mark (depending on whether 10-90% or 20-80% rise time is measured) is later than the end of the baseline by more than a half of the baseline duration (1 ms in our case), a new baseline is established closer to the peak (by moving the baseline to the next local minimum).
15. Finally, the amplitude range test is applied again (Step 9).
16. A mini (mPSP/mPSC) is established.

Detection using MiniAnalysis software

MiniAnalysis software version 6.0.7 was used to detect mEPSPs for a benchmarking purpose. We used the following detection parameters: As with the 'minis' program, an amplitude threshold of 0.1 mV (when constructing the full ROC-like curve) or 0.05 mV (all other simulated conditions), in both cases somewhat matched to the simulated data, or 0.01 mV when detecting real minis, a "Period to search for a Local maximum" of 12.5 ms, "Time before a peak for baseline" of 10 ms, a "Period to search a decay time" of 30 ms, a "Fraction of peak to find a decay time" of 0.37 (one effective time constant for exponential decay), a "Period to average a baseline" of 2 ms, an "Area threshold" of 0 mV×ms (i.e., not used), a "Number of points to average for peak" of 1, and using the "Detect complex peak" option (to avoid missing close-together events). The chosen detection parameters closely resembled similarly named parameters in the 'minis' detection algorithm with minor deviations to improve performance. Arrived by trial and error, these parameters were also found to give the most optimal detection performance of the MiniAnalysis software in comparison to other tested parameter sets. Event detection was carried out on the recording data that was filtered and smoothed in the same way as described in steps 1 and 2 of the previous sub-section (Figure 2).

Detection using Clampfit

376 Clampfit software, part of the pClamp 11.0.3.03 software suite, was used to detect real and
377 simulated mEPSPs and mEPSCs for a benchmarking purpose. Recordings were band-stop filtered as
378 described in step 1 of the 'minis' detection algorithm. Data was not smoothed. A template search
379 algorithm was used with 9 templates. The mEPSP template set was constructed based on the
380 simulated events. Events having 0.5 ms, 1.5 ms, 3.5 ms, and 6.5 ms 10-90% rise times were selected
381 to produce 4 distinct mEPSP templates (with the correct decay time constants). An additional 5
382 single-peaked templates were constructed in a way that made them potentially a mix of multiple
383 simulated waveforms. They were constructed to have extra-fast, fast, intermediate, slow, and extra-
384 slow rise times corresponding to 2 ms, 2.75 ms, 6 ms, 7 ms, and 8 ms 0-100% rise times and 8 ms,
385 9.25 ms, 17 ms, 23 ms, and 37 ms duration full decays, respectively. Combining single and mixed
386 waveforms gave better detection performance than having waveforms based only on any one of
387 these types alone. Template match threshold was set to the default of 4 noise standard deviations
388 with the rest of the detection parameters being set to their default values as well. The same set of
389 templates was used to analyse all simulated current clamp data, as well as real data. Using the same
390 templates with real data was justified, because they resulted in a superior detection performance
391 compared to templates created directly from the real data.
392
393 *Detection algorithm response classification*
394 At the outset we identified prominent noise events in the V_m noise recordings (the 2nd recording
395 phase: 'noise-alone' condition) that could potentially be confused for true minis (mEPSPs) by any of
396 the algorithms (noise traces in Figures 2A and B). All noise recordings were filtered and smoothed as
397 in Steps 1 and 2 of the 'minis' detection algorithm (Figure 2). The data was further smoothed by a
398 rectangular 'box-car' moving average window of 20 ms. Then all peaks larger than 0.01 mV and
399 having a half-width of at least 0.5 ms were identified. These peaks were classed as (notional) noise
400 'events' (for the purpose of generating 'sensible' true negative rates, TNRs, which do not 'swamp'
401 false positive rates across the entire virtual ROC; see below). Subsequently we simulated mEPSPs

402 and added them at pseudo-random times to a zero-trace having the same length as the noise
403 recording of interest (Simulation traces in Figures 2A and B). The peaks of these events were classed
404 as signal events. The simulated trace was then added to the noise recording ("Simulation + noise"
405 traces in Figures 2A and B). Locations of signal and designated noise events formed the 'ground
406 truth' information.
407
408 Following the detection process, all detected events were associated with one of the signal and
409 noise events depending on their proximity to these predefined 'ground truth' events. A detected
410 event was classed as a true positive (a 'hit') if it was the closest detection event within 5ms of a
411 signal (simulated mEPSP/mini) event. If no detection event occurred within the 10 ms symmetrical
412 window surrounding a signal (simulated mini) event (-5 to 5 ms), the signal event was classed as a
413 false negative (a 'miss'). If no detection event (except correct detections) occurred within the same
414 duration window surrounding a noise event, the noise event was classed as a true negative ('correct
415 rejection'). Although in theory there could potentially be a much higher number of possible time
416 points which could be labelled as correct rejections, or true negatives, in this situation, because of
417 their inherently somewhat arbitrary nature, we wanted to keep the maximum number comparable
418 to the maximum number of true positives (simulated minis), so the ROC plot had a reasonable
419 chance of being relatively 'square' (i.e. having a useful dynamic range). The remaining detection
420 events were classed as false positives ('false alarms'). Examples of classified detection events are
421 shown in Figure 2 separately for all three detection algorithms.
422
423 *Detection response time to the nearest neighbour*
424 The time to the peak of the nearest smEPSP was available for every classified response. Detection
425 performance was then evaluated as a function of the time to the nearest neighbour.
426
427 **Membrane potential 'phase' (trend) classification**

428 We attempted to address common detection errors, in particular missed minis on the decaying
429 phase of a previous mini (causing second peak to drop relative to its baseline), or on the rising phase
430 of another mini (so the rises of both minis get lumped together). Algorithm detection performance
431 was assessed not only for full recordings but also separately for periods when the 'underlying'
432 simulated V_m (before adding the noise) was rising, decaying, or remained roughly stable (Figure 3).
433 The 'decaying phases' (downward trend) of the purely simulated V_m were set to be a) the period
434 from 0.0625 ms after the peak until the purely simulated V_m trace dropped to the ratio of 0.3/e mV
435 (0.11 mV) (amplitudes of simulated minis were ~0.3 mV in the full virtual-ROC curve conditions, so
436 this would be about one membrane time constant after an 'average' simulated mini) or b) until the
437 V_m started rising again to reach a new peak that was above the initial peak (at the start of this decay
438 phase). If the new peak was lower than the initial one, the entire new peak was classified as part of
439 the ongoing decay phase. Peaks occurring on the decay phase of the V_m were assigned the V_m decay
440 rate of change that was present 0.25 ms (5 sample points) prior to the appearance of the V_m
441 inflection points associated with the start of the rise of a new mini (indicated by the blue arrow in
442 Figure 3A). The rising 'phase' was treated essentially somewhat as a decay phase in reverse. The only
443 difference was that the ratio of 0.3/e mV was replaced by the ratio of 0.3/10 mV (0.03 mV). Peaks
444 occurring on a V_m rise phase (upward trend) were assigned a V_m rate of rise value that was present
445 0.125 ms *after* the appearance of an upward V_m inflection point following the initial decay of the
446 previous peak (indicated by green arrows in Figure 3A). Periods that were already classified as decay
447 phases could not be reclassified as rising phases. Periods of relatively slowly-changing simulated V_m,
448 outside of the rise and decay phases were classed as "stable" (or a flattish phase). The classification
449 of purely simulated membrane potentials into three different trend phases was used to assign
450 phases to the combined noise recordings + simulated minis (Figure 3B). The detection performance
451 during rise and decay trend phases was evaluated as a function of the V_m rate of change.
452
453 **Data Analyses**

Performance of the three algorithms was compared using measures from signal detection theory. All detection responses were classified as described in the *Detection algorithm response classification* subsection. True positive ('hit') rate (TPR) was calculated as follows:

$$TPR = \frac{True\ positive\ count}{True\ positive\ count + False\ negative\ count}.$$

Throughout this text we use TPR, detection probability, and sensitivity interchangeably. False positive ('false alarm') rate (FPR) was calculated as follows:

$$FPR = \frac{False\ positive\ count}{False\ positive\ count + True\ negative\ count}.$$

The true negative count we have used is perforce notional, as explained above, but still useful for standardised, non-subjective comparisons and benchmarking. Throughout we use FPR and 'false alarm rate' interchangeably.

Calculation of TPR and (notional) FPR allowed us to produce ROC-like curves and to calculate area under the curve (AUC; area under the ROC curve, for each complete ROC curve, with 0.5 indicating chance performance (the area of the triangle under the diagonal from (0,0) to (1,1) and 1 indicating perfect performance, i.e., the area of a right angle starting at (0,0), vertical to (0,1) then going horizontal to (1,1)) as detection performance indicators. These are the most commonly used performance indicators for classifiers, in addition to sensitivity (TPR), and d' (discriminability or sensitivity index) which we often use in parallel throughout this text. The d' statistic was calculated as follows:

$$d' = z(TPR) - z(FPR),$$

where z is the z-score defined as the inverse of the normal cumulative distribution function, i.e. z(arg) is the number of sd's from the mean giving the area equal to its argument arg under the standard unit normal distribution (mean 0, sd 1), starting from -∞. TPR and FPR values are essentially

treated as cumulative probabilities as explained in (Macmillan and Creelman, 2005). So, d' tells us how many standard deviations 'apart' the TPR and FPR are, assuming they are cumulative probabilities (areas under curve) of a standard normal distribution. N.B. If FPR is 0, z(FPR) is -∞ so d' is undefined, but arbitrarily large and positive (as occurs in some of our figures below). These plots are truncated for the detection method in question, but the performance is still superior to any plots with finite values.

The above detection performance indicators were calculated for full recordings, as well as separately for rising and decaying periods of V_m.

In addition, we also looked at cumulative (left-to-right over the x-axis) TPR and cumulative FPR. The cumulative TPR was defined as follows, for each detection algorithm and simulated waveform:

$$Cumulative\ TPR = \frac{Cumulative\ true\ positive\ count}{Total\ unbanded\ true\ positive\ count} * Overall\ unbanded\ TPR.$$

Likewise, the cumulative FPR was defined as:

$$Cumulative\ FPR = \frac{Cumulative\ false\ positive\ count}{Total\ unbanded\ false\ positive\ count} * Overall\ unbanded\ \ FPR.$$

The latter two measures were not only useful for measuring cumulative hits and false alarms over a range of time intervals and V_m rates of change, but also provided overall estimates of TPR and FPR (the right side of the x-axis).

Statistical analyses

All inferential statistics were based on the assumption that distributions of all measures were normal. Only repeated samples or single-sample (often when comparing with baseline true positive values in tables) t-tests were used across the Results section. All mean distribution values are stated/depicted with 95% confidence limits of the mean (if exist).

504 **Data accessibility**

505 All data analysed in this study is publicly available (GIN DOI). The available data include 'noise +
506 minis' and 'noise-alone' whole-cell patch membrane potential recordings that were used in minis
507 detection procedures and computer simulations. The hybrid V_m traces containing smEPSPs added to
508 noise recordings are also available. All electrophysiological recordings were stored in Axon Binary
509 File (ABF) format.

510

511 mEPSP templates used for detecting real and simulated events via Clampfit are also in the same
512 dataset in the form of Axon Template Files (ATFs).

513

514 **Code accessibility**

515 All analyses were carried out in Matlab and the analysis code is publicly available on GitHub
516 (available once published). The code is complete with instructions on how to reproduce all figures
517 reported in this study.

518

519 **Software accessibility**

520 The present study reported the use of a novel mEPSP/mEPSC detection algorithm that is part of
521 'minis' software available on GitHub (Dervinis, 2022).

522

Results

Research literature measuring minis in the central nervous system

The full results of the literature survey are reported in Supplementary Results. Here we only briefly report key findings. First, we established that the two most popular software applications used to detect minis are MiniAnalysis followed by Clampfit with 48% and 26% of surveyed studies reporting to use these algorithms, respectively. Moreover, these studies reported a mean minis' incidence rate of 3.6 ± s.d. 0.34 per second (range of 1.0 to 8.0 per second). Meanwhile, we suspect that true minis incidence rates range somewhere between ca. 10 minis/s and 100 minis/s based on research on synapse counts and release probabilities in the CNS (an order of magnitude higher than reported direct measurements using voltage clamp).

Algorithm performance comparison for detecting moderately-sized (~0.3 mV) simulated miniature excitatory postsynaptic potentials

Detection under a wide range of incidence rate conditions: overall performance

In the Results subsection 'Research literature measuring minis in the central nervous system', we reported that detection of spontaneous postsynaptic events is typically carried out using an amplitude threshold. This approach implies that the range of amplitudes of spontaneous postsynaptic events is somewhat known and that, on the smaller end, the amplitudes are moderately-sized and sufficiently larger than pure noise fluctuations. Leaving aside the question of the empirical validity of this (somewhat dubious?) assumption, we evaluated automated detection of moderately-sized (0.3 ± s.d. 0.05 mV) smEPSPs added to whole-cell patch clamp noise recordings (the 2nd recording phase: 'noise-alone' condition).

We compared our novel 'minis' algorithm with MiniAnalysis and Clampfit. We created 14 simulation incidence rate conditions with different effective signal-to-noise ratios that loosely mimicked the

548 effects of varying the signal detection threshold. On the one hand, increasing the incidence rate of
549 smEPSPs tended to decrease TPR as simulated events started to merge. On the other hand,
550 increasing the noise amplitude (scaling up the noise that was added to the simulated minis) tended
551 primarily to increase the FPR.
552
553 We plotted the detection performance in terms of TPRs against FPRs, as 'virtual' (notional) Receiver
554 Operator Characteristic (v-ROC) curves, for all 14 conditions and all three algorithms in Figure 4A.
555 We found that in the first six conditions (high minis incidence rates), the v-ROC curve for 'minis' had
556 minimal overlap with any other curve and was positioned furthest away from the diagonal (starting
557 from left to right; 640, 320, 160, 80, 40, and 20 minis/s with x1 noise scaling), indicative of a superior
558 performance in this (relatively high) incidence rate range (the highest incidence rates were used to
559 create the full v-ROC; higher incidence rates increase overlaps, i.e. temporal summation, between
560 minis, which are particularly challenging to detect). The same observation was supported by another
561 measure, the sensitivity index d', shown in Figure 4B. Detection performance in the remaining 8
562 conditions (10, 5, 2.5, 2.5, 2.5, 2.5, 2.5, and 2.5 minis/s with noise scaling factors of x 1, 1, 1, 1.2, 1.4,
563 1.8, 2.6, and 4.2, respectively) was very similar for both 'minis' and MiniAnalysis: neither of the two
564 showed a clear superiority on both performance measures simultaneously: v-ROC and d' curves
565 overlapped. In contrast, Clampfit consistently performed worst across all 14 conditions, particularly
566 with high amplitude noise. Clampfit becomes progressively 'confused' as noise increases, placing
567 templates on noise events, but ignoring 'swamped' smEPSPs.
568
569 When overall performance was assessed averaging across individual incidence rate and signal-to-
570 noise ratio conditions, we found that 'minis' showed the best performance with the mean Area
571 Under the (v-ROC) Curve (AUC) value of 0.960 ± 0.002 (95% confidence interval here onwards; Figure
572 4C). A paired samples t-test comparing to MiniAnalysis which had a mean AUC value of 0.937 ±
573 0.0022 gave $t(13) = 12.4$ and $p = 1.37\times10^{-8}$. Clampfit showed the poorest overall performance with

574 the mean AUC value of 0.706 ± 0.0043, t(13) = 33.1, and p = 6.14×10^{-14} when compared to the
575 MiniAnalysis mean AUC value in a paired samples t-test. These differences in detection performance
576 were further corroborated by the d' measure averaged across all signal-to-noise ratio conditions
577 (Figure 4D). A paired samples t-test comparing mean d' values from 'minis' (2.45 ± 0.045) versus
578 MiniAnalysis (2.11 ± 0.04) gave t(13) = 14.0 and p = 3.24×10^{-9}. The same test comparing the mean d'
579 from MiniAnalysis and Clampfit (1.23 ± 0.024) gave t(13) = 13.3 and p = 6.07×10^{-9}. In summary, these
580 findings clearly demonstrated that our 'minis' detection algorithm outperformed the other two
581 algorithms, for ~0.3 mV simulated minis added to real recording noise, at incidence rates above 10
582 minis/s, while Clampfit consistently showed the poorest detection performance across the entire
583 incidence rate and signal-to-noise range examined, for these mPSP shapes and templates.
584
585 *Detection under a wide range of incidence rate conditions: common errors*
586 Both 'minis' and MiniAnalysis were fairly good at detecting moderately-sized (0.3 ± s.d. 0.05 mV)
587 smEPSPs added to our noise-alone recordings. Yet all three algorithms, including 'minis', missed a
588 sizeable proportion. Figure 5 shows examples of common mistakes. One type of mistake was missing
589 simulated events that occurred very close to other events (Figures 5A, B, C, D, E, F, and G).
590 Unsurprisingly, none of the three algorithms could deal with events that overlapped nearly perfectly,
591 always lumping them together. Detecting peaks in the data using thresholds or fitting templates to
592 the data cannot offer a way of identifying overlaps. Another common error type was missing events
593 with peaks on the rising phase of another mEPSP (Figures 5A, B, C, D, E, and F; green arrowheads).
594 Unlike perfect or near-perfect overlaps, these events had a clear but brief decay period that was
595 quickly upended by the rising phase of the next mini. Because these decays were brief, they were
596 often lumped with a subsequent mEPSP or they could not be adequately fit with a template by
597 Clampfit and, therefore, were discarded. The 'minis' program (but not MiniAnalysis) does offer a way
598 to minimise these errors by reducing the peak integration period, but this comes at the expense of
599 noise fluctuations on the rising phase increasingly passing as postsynaptic potentials (a type of false

600 positive; Figure 5H, red arrowheads). An effective solution to this problem would, therefore, require
601 isolating and measuring the noise component in whole-cell patch clamp recordings - which currently
602 is not implemented in either MiniAnalysis or Clampfit (but is in 'minis').
603
604 An even more common error type was to miss (smaller) mEPSPs that occurred on the decay phase of
605 another, often larger, earlier mEPSP (Figures 5D and G; blue arrowheads). The amplitude of mEPSPs
606 occurring on decays is effectively reduced (as the peak drops relative to the baseline, due to the
607 underlying decay of V_m) and the steeper the decay, the more the amplitude is reduced. The
608 amplitude of such a reduced mini may fall below the detection threshold and/or shape distortions
609 may prevent fitting a template. As a result, such mEPSPs were occasionally discarded (this turns out
610 to be a significant problem with real minis recorded from cortical pyramidal neurons, which exhibit
611 significant temporal summation, because of their relatively high incidence rates and slow decays).
612 There is no easy way of correcting these errors, as it would (for example) require estimating the
613 underlying decaying potential and subtracting it from the overall V_m or estimating the fall in the peak
614 and adding it back to the amplitude before deciding whether to accept that candidate putative mini.
615 mEPSPs that neither occurred during the rise nor decay phases were also occasionally missed
616 (Figures 5A, D, E, and F; black arrowheads). This could have happened due to a failure to fit a
617 template (Clampfit) or due to the amplitude being reduced below threshold by *downward*
618 background noise fluctuations. In recordings of real mEPSPs, these errors would mainly affect small
619 amplitude mEPSPs. Again, an effective solution to this problem would require isolating and
620 measuring the noise component in whole-cell patch clamp recordings similarly to previously
621 discussed errors occurring on the V_m rise phase.
622
623 A whole other class of detection errors appeared in the form of false alarms (false positives)
624 occurring on the rising (Figure 5E; red arrowhead) or decaying phases (Figures 5A, B, and H; red
625 arrowheads) of underlying mEPSPs or in the absence of any other minis in the vicinity (Figures 5B

626 and H; red arrowheads). These mistakes were often caused by *upward* background noise
627 fluctuations passing as real minis and might have been 'enabled' by low amplitude detection
628 thresholds or an inability to discern shapes of real minis from mini-like noise. Just like the previously
629 discussed error type, a solution would require isolating and measuring properties of the noise
630 component. In addition, there were errors that uniquely affected only one of the algorithms, like the
631 misplacement of detected events (peaks) by MiniAnalysis (Figure 5C; green arrowheads).
632
633 We saw that distinct detection errors could be made depending on how close they were to
634 neighbouring mEPSPs and whether they occurred on the rise or decay phases of other nearby
635 mEPSPs or in the absence of any other mEPSPs in the background. All three algorithms occasionally
636 committed these errors, but their incidence was uneven.
637
638 *Detection under a wide range of incidence rate conditions: the membrane potential 'slope trend'*
639 *effect*
640 In order to quantify the detection performance in different circumstances, for the same ~0.3 mV
641 smEPSPs, we evaluated the probability of making errors in relation to the *proximity* to neighbouring
642 minis and the phase (*trend*) of the background V_m: rising or decaying. We looked at TPR as a function
643 of time interval to the nearest-neighbour mini (Figure 6A) taken together for all minis incidence rate
644 conditions used above (but excluding conditions where noise was scaled): i.e., 640, 320, 160, 80, 40,
645 20, 10, 5, and 2.5 minis/s conditions (9 in total). We found that detection was superior for our 'minis'
646 program across the entire inter-mini interval range. MiniAnalysis came second, with Clampfit
647 consistently worst. These differences in detection performance were also reflected in the *cumulative*
648 TPR (Figure 6D). As for the FPR (Figure 6B), 'minis' was superior at detecting ~0.3 mV smEPSPs that
649 were within 10 ms of the nearest neighbour (peak-to-peak). This performance edge over
650 MiniAnalysis was not maintained for larger inter-mini peak intervals, while Clampfit again showed
651 consistently the worst performance across the entire interval range. These performance differences

652 were also reflected in the *cumulative* FPR (Figure 6E). Taken together, true and false positive rates
653 allowed as to calculate a combined performance indicator, sensitivity index d', as a function of time
654 to the nearest neighbour (Figure 6C). The combined measure indicated that 'minis' had the superior
655 detection performance within 10 ms of the nearest neighbour while Clampfit showed the worst
656 performance across the entire inter-mini interval range.
657
658 During the V_m rise phase performance differences were unequivocal. There were very few events
659 and, therefore, positive detections when the background V_m was rising at 200 µV/s or faster (Figure
660 7D). Most of the detected events coinciding with the rise phase actually occurred when V_m was
661 changing at the rate of 10 to 100 µV/s. In this range 'minis' showed the best detection performance
662 with d' between 1 and 2 (Figure 7C). MiniAnalysis was the second best, while Clampfit showed the
663 worst performance. This order of performance was maintained for rates below 10 µV/s with overall
664 performance improving for all algorithms. The performance edge of 'minis' over the other
665 algorithms was primarily due to low FPR (Figure 7B). The TPR of 'minis' was also superior to the
666 other two algorithms but, in terms of sensitivity, MiniAnalysis was not far behind (Figure 7A). In the
667 range between 15 and 35 µV/s 'minis' actually fell slightly behind MiniAnalysis. The cumulative rates
668 clearly supported the observation that 'minis' was superior to the other two algorithms with
669 MiniAnalysis coming second and Clampfit having the worst performance (Figures 7D and E).
670
671 The same behaviour of the three algorithms was also observed for detecting ~0.3 mV smEPSPs
672 occurring on the decay phase of the background V_m (caused by summation of other smEPSPs). Most
673 of the detected simulated events were associated with rates of V_m change in the range of -100 and -
674 10 µV/s (Figure 8D). In this range and above, 'minis' demonstrated the best performance relative to
675 the other two algorithms with d' ranging between 1.5 and 2.5 (Figure 8C). MiniAnalysis again came
676 second, while Clampfit showed very poor performance. Clampfit often had a d' that was close to 0,
677 meaning that its performance was often not different from chance level when background V_m was

678 decaying. This was mainly due to the large FPR for this algorithm (Figure 8B); 'minis' had
679 unequivocally the highest TPR and the lowest FPR (Figures 8A and B) with cumulative rates very
680 clearly reflecting this (Figures 8D and E). The overall performance of the runner-up, MiniAnalysis,
681 was substantially poorer.
682
683 There are only 3 conditions with realistic incidence rates (20, 40, and 80 minis/s). Although, higher or
684 lower incidence rates were useful in constructing the full v-ROC curve, it can be argued that they are
685 artificial and experimental electrophysiologists may not be concerned with them. Therefore, we also
686 examined the membrane potential 'slope trend' effect separately for the three realistic incidence
687 rate conditions in the Supplementary Results section demonstrating similar findings to the overall
688 results.
689
690 **Algorithm performance comparison for detecting simulated excitatory postsynaptic potentials**
691 **with a wide set of discrete amplitudes, at realistic incidence rates**
692 So far, we have only tested performance of the three algorithms when detecting moderately-sized
693 (0.3 mV ± s.d. 0.05 mV) mEPSPs with a relatively narrow range of amplitudes. The existing evidence
694 does not indicate that either mPSPs or mPSCs form a distinct amplitude distribution that can be
695 separated from the amplitude distribution of noise fluctuations. Therefore, here we aimed to test
696 the performance of detecting smEPSPs of a wide range of amplitudes, to evaluate the three
697 algorithms in more realistic settings.
698
699 We used three incidence rate conditions: 27, 38, and 61 minis/s. Within each of these conditions
700 smEPSPs were drawn pseudo-randomly from a uniform distribution of the following ten discrete
701 amplitudes: 0.05, 0.1, 0.15, 0.2, 0.25, 0.3, 0.35, 0.4, 0.45, 0.5 mV (4 different simulations per noise
702 trace per incidence rate conditions; see Methods for shapes). Just like in previous simulations, we
703 positioned these smEPSPs pseudo-randomly over noise recordings and detected them using the

704 three algorithms. The overall performance of these algorithms is shown in terms of true and false
705 positive rates in Figure 12A and d' in Figure 12B. A few things are prominent in these graphs. First of
706 all, the detection performance of all algorithms was considerably worse than when detecting
707 moderately-sized (~0.3 mV) mEPSPs. Secondly, 'minis' again had the edge over two other algorithms,
708 especially at higher minis' incidence rates. Third, Clampfit's performance was consistently the
709 poorest, in our hands.
710
711 Performance was also assessed pooling the incidence rate conditions. We found 'minis' to have the
712 best performance with the mean AUC value of 0.827 ± 0.003 (95% confidence interval from here on;
713 Figure 12C). A paired samples t-test comparing to MiniAnalysis with the mean AUC value of 0.809 ±
714 0.003 gave $p = 1.0\times10^{-6}$. Clampfit showed the poorest performance, with the mean AUC value of
715 0.665 ± 0.004, $p = 2.2\times10^{-10}$ when compared to the MiniAnalysis mean AUC value in a paired samples
716 t-test. These differences in detection performance were further corroborated by the d' measure
717 averaged across all incidence rate conditions (Figure 12D). The d' discriminability index scores of
718 'minis' (1.5 ± 0.05) and MiniAnalysis (1.33 ± 0.04) were significantly different ($p < 10^{-5}$), as were the
719 d' from MiniAnalysis and Clampfit (0.61 ± 0.02) ($p < 4\times10^{-6}$) The conclusion based on combined
720 measures was in line with the assessment based on Individual incidence rate conditions.
721
722 Other measures like true positive and false positive rates as functions of the interval to the nearest
723 neighbour and V_m rate of change during the rise or decay phases using more realistic settings
724 pointed to a very similar conclusion to that made with the full virtual ROC curve. First, we found that
725 'minis' performed better than the other algorithms at detecting mEPSPs that were within 10 ms of
726 other mEPSPs, and that at larger intervals, MiniAnalysis performed just as well (Figure 13).
727 Meanwhile, Clampfit performed consistently the worst across the range of inter-mini intervals
728 whether in terms of d' (Figure 13C) or true and false positive rates (Figures 13A, B, D, and E). When it
729 came to V_m rate of change, 'minis' performed better than MiniAnalysis, which in turn performed

730 better than Clampfit when detecting smEPSPs occurring during rise and decay phases of background
731 simulated V_m (Figures 14 and 15). One difference compared to the full virtual ROC curve analysis was
732 that the detection performance of 'minis' and MiniAnalysis overlapped in the range of 15-25 µV/s
733 when detecting smEPSPs occurring on the rise phase of the background V_m (Figure 14C). This is
734 largely caused by an increased FPR of 'minis' in this rate range (Figure 14B). The overall performance
735 of all algorithms was better (Figures 14C and 15C) compared to the full virtual ROC curve analysis
736 (Figures 7C and 8C), but still worse when compared to detecting moderately-sized (~0.3 mV)
737 smEPSPs with realistic incidence rates (Figures 10C and 11C), as described in the previous
738 subsection. In summary, 'minis' had a substantial advantage when detecting minis in close proximity
739 to neighbouring minis, as well as during rising or falling background V_m, with Clampfit severely
740 underperforming.
741
742 **Comparison of amplitudes, time course, and incidence rates of detected real and simulated**
743 **excitatory postsynaptic potentials by different algorithms**
744 In the final section we looked at how the three tested algorithms fare across all simulation
745 conditions in terms of their minis' amplitude, time course, and incidence rate estimates. We also
746 carried out detection of real minis in the same recorded cells prior to blocking minis ('noise + minis'
747 condition) and compared the same estimates for the three algorithms. A large number of estimates
748 and inferential statistics was compiled into several tables providing a thorough performance
749 overview.
750
751 Table 1 below shows the compiled mean amplitude estimates for simulated and real minis detected
752 by the three algorithms while Table 2 shows repeated samples t-test p-values for all possible
753 comparisons of mean amplitude values for the three different algorithms as well as ground truth
754 values. Mean amplitude values of simulated and real mPSPs detected by 'minis' were consistently
755 lower than mean amplitude values of events detected by both MiniAnalysis and Clampfit and were

closest to ground truth values as indicated by p-values of corresponding comparisons. Detection of simulated events by 'minis' algorithm in conditions with realistic smPSP incidence rates (i.e., Type 1 RI and Type 2 rows in the tables) were extremely close to the ground truth values (0.3 mV vs 0.31 mV and 0.275 mV vs 0.29 mV, respectively; Table 1). These observations further confirm that 'minis' detection algorithm is exceptionally good at picking small PSPs. The tendency to overestimate amplitudes of detected smPSPs in high incidence conditions (i.e., Type 1 HI row in the tables) by all three algorithms reflects the increased probability of major overlap between simulated events in these conditions.

Table 3 below shows the compiled mean 10-90% rise time estimates for simulated and real minis detected by the three algorithms while Table 4 shows repeated samples t-test p-values for all possible comparisons of mean 10-90% rise time values for the three different algorithms as well as ground truth values. All three algorithms tended to significantly overestimate the rise times of detected minis in all simulated conditions. This can be explained by the fact that noise fluctuations affect the baseline positioning by shifting it to the lowest trough some time prior to the real start of the event. The rise times of detected events are also more likely to be overlaps of more than a single event and, therefore, would tend to be longer if lumped together. This was especially true for events detected by Clampfit which had a pronounced tendency to lump smaller events into fewer bigger ones. Both MiniAnalysis and Clampfit had large range values. For example, MiniAnalysis had a range of 0.02-18 ms and Clampfit had a range of 0.09-37 ms when detecting real mPSPs, while 'minis' had a range of 0.35-9.4 ms when detecting the same type of events (Table 3). This observation is indicative of the fact that MiniAnalysis and Clampfit occasionally failed to accurately position the baseline of a detected event and failed to reject 'wildly' inaccurate estimates.

Table 5 below shows the compiled mean 1/e decay time estimates for simulated and real minis detected by the three algorithms while Table 6 shows repeated samples t-test p-values for all

782 possible comparisons of mean decay time values for the three different algorithms as well as ground
783 truth values. Decay times of smPSPs detected by 'minis' were the closest to the ground truth values
784 when compared to the other two algorithms as evident by comparing t-test p-values in Table 6. For
785 simulated realistic incidence rate conditions (i.e., Type 1 RI and Type 2 rows in the tables) p-values
786 were not significant for the 'minis' vs the ground truth comparison (Table 6). Unfortunately, the
787 same cannot be said of MiniAnalysis and pClamp which consistently overestimated or
788 underestimated mean decay times, respectively (Tables 5 and 6). These differences between the
789 algorithms may stem from differences in how decays are being estimated: Whether effective decays
790 are measured or detected events are fitted with exponential decay functions. 'Minis' reduce these
791 discrepancies by averaging the two methods to obtain a single estimate.
792
793 Table 7 below shows the compiled mean incidence rates for simulated and real minis detected by
794 the three algorithms while Table 8 shows repeated samples t-test p-values for all possible
795 comparisons of mean incidence rates for the three different algorithms as well as ground truth.
796 Values produced by 'minis' and MiniAnalysis were close to each other as well as ground truth values
797 (albeit less so for MiniAnalysis) as indicated by corresponding p-values of the t-test statistic (Tables 7
798 and 8). Incidence rate values produced by Clampfit were considerably lower than the other two
799 algorithms or the ground truth values indicating that Clampfit missed many events, as well as tended
800 to lump events together. A distinct ability by 'minis' algorithm to pick up smaller events was further
801 supported by a considerably larger incidence estimate for real data when compared with the other
802 two algorithms. Clampfit values for real data were smaller by almost an order of magnitude
803 revealing a really poor performance by this algorithm.
804

Discussion

Our analysis suggests that mini (mEPSC/P) incidence rates typically reported in neocortical slices in the CNS synaptic function literature may be underestimated, by up to an order of magnitude. Discrepancy of this size indicates that signal-to-noise ratio is a severe issue preventing accurate detection of minis irrespective of the detection method used: That is, both 'template matching' and 'thresholded amplitude detection' approaches are significantly flawed in distinguishing real minis from the background physiological noise. Having stated that, however, we also demonstrated that the two approaches are not equally flawed and that 'thresholded amplitude detection' performs reasonably well and is further improved by our novel mEPSC/P detection algorithm called 'minis'.

We quantified the performance of 'minis' using standard measures from signal detection theory – namely, ROC (receiver operating characteristic) curves and sensitivity index d', alongside measures of sensitivity – true positive rate (TPR) and false positive rate (FPR = 1 – specificity) – and demonstrated superior performance of our algorithm relative to the other two most popular algorithms in the field of minis research: MiniAnalysis and Clampfit. Our algorithm had a performance edge over the other two algorithms not only for detecting moderately-sized (~0.3 mV) mEPSPs, but also across a wide range of realistic mEPSP amplitudes, shapes and incidence rates. Crucially, the latter included the higher minis' incidence rates observed in neocortical slice experiments at body temperature, 13-80 minis/s, where temporal summation becomes an increasing challenge for detection. As a necessary step in building a reliable quantal size estimation method, we succeeded in developing an algorithm for detecting postsynaptic events that is transparent, systematically evaluated, and flexible.

Notwithstanding its good performance, the 'minis' algorithm has important limitations. First, the 'minis' algorithm, just like the other two detection algorithms, cannot by itself alone be used to

830 estimate quantal sizes. Due to amplitude attenuation of spontaneous postsynaptic events and the
831 need to use amplitude detection thresholds, the estimated amplitude will generally only be an upper
832 limit on the actual population mean amplitude. We have also demonstrated that mini detection is
833 impaired on rising and decaying trends of V_m. The severity of this problem worsens with the rate of
834 change of V_m. The problem is exacerbated as the time between neighbouring minis gets shorter.
835 Therefore, the mean amplitude estimate is not only affected by the presence of noise and by
836 amplitude attenuation, but also by the presence of other miniature postsynaptic events. All the
837 above limitations also apply to estimating the incidence rate of postsynaptic events. All the
838 mentioned factors reduce event detectability and, therefore, result in an underestimated incidence
839 rate. However, 'detecting' noise events as false minis can cause errors in the other direction if too
840 low a detection threshold is set. Despite these limitations, our program 'minis' fares better on this
841 front compared to the other two algorithms: 'minis' performance is also superior on rising and
842 decaying trends in V_m, and for closely-spaced events. To our knowledge, this is the first time these
843 problems have been addressed, and their impact quantified in a systematic manner, and their
844 implications discussed.
845
846 Other caveats concern the method for assessing the performance of detection algorithms. We did
847 not use the full plausible range of realistic distributions for simulating mEPSPs in terms of their
848 incidence rates, amplitudes, and their rise and decay times. However, the shapes of these
849 distributions are not entirely known, and this is an empirical question that remains unanswered.
850 Because of this reason, we refrained for trying to address this question here and avoided making
851 empirically dubious assumptions. Instead, we explored a range of scenarios where simulation
852 incidence rates ranged from more to less realistic. We explored the effects of varying signal/noise
853 ratios. We believe that the large size of the parameter space we have explored does allow us to
854 conclude that the three algorithms differ systematically in their performance, with our algorithm –
855 'minis' – being superior to the other two (in our hands at least).

We have not constructed ROC curves in the usual fashion by varying a detection threshold of each algorithm. Unfortunately, we were limited by the nature of the algorithms, specifically Clampfit which does not use a pure amplitude detection threshold but uses convolution of the data trace with each of the templates. However, our manipulations of varying the incidence rate of simulated events, as well as varying the amplitude of noise, allowed us to mimic effects of varying the detection threshold. We are also aware of one particular issue regarding the classification of correct rejections (true negatives). One could argue that a proper definition of correct rejections would require treating every data sample point as a potential noise event that could either be falsely detected as a signal event or correctly rejected as a noise event. Unfortunately, such a definition would result in large numbers of correct rejections (true negatives) swamping the number of other detection measures (true positives, false alarms (false positives), and misses (false negatives)) and, therefore, would make the detection performance analysis essentially meaningless. Alternatively, treating every 10 ms noise window as a basis for correct rejection would still produce a relatively large number of correct rejections, as would similar, more complicated schemes. There is also no reason why a single noise event should be limited to a single 10 ms window. Therefore, we thought that a reasonably practical definition of correct rejections as rejected prominent noise fluctuations fared better than the alternatives. Having explicit, transparent, and reproducible, methods to benchmark the performance is better than relying on subjective examination of recording traces.

Finally, we would like to address the question of whether we used optimal detection settings for each algorithm. MiniAnalysis settings were similar to those of ‘minis’. The two algorithms are somewhat similar and chosen settings were observed to give the best performance for both algorithms when detecting simulated mPSPs, after considerable exploration. In case there is any doubt about our method, we have made our recorded and simulated data and Matlab analysis code publicly available. With regards to using Clampfit to analyse simulated data, we used 9 templates

882 (the maximum allowed) constructed in a typical fashion by averaging a number of waveforms with
883 similar shapes but separating qualitatively different shapes. These templates have also been made
884 available publicly. We tested different detection regimes with templates based on both smoothed or
885 unsmoothed traces and comparing detection of smoothed and unsmoothed recording traces and
886 chose the best regime. However, we did not construct new templates for every new recording or
887 every new simulation condition, because this is extremely time-consuming and is not an efficient
888 way to conduct this type of analysis, although Clampfit detection performance might have improved
889 marginally. Clampfit might perform better if the number of templates was not limited to 9, and if a
890 wide range of inbuilt templates was available. These issues are, however, outside the scope of this
891 study. Given these considerations, we are confident in the validity of our approach.
892
893 We defer the discussion of reasons why there is such a big discrepancy between reported and
894 expected minis' incidence rates in the synaptic physiology literature and how they can be effectively
895 addressed to our companion article. It is worth noting, however, that 'minis' or another similar
896 algorithm can be used to objectively measure the properties of pure noise fluctuations (with minis
897 blocked). This would allow one, in principle, to separate 'signal' (minis) from noise components in
898 traces of minis recorded in the presence of noise. Noise events could potentially be 'removed' from
899 the combined signal and noise event distribution by direct histogram subtraction, although in
900 practice it turns out one needs to compensate for the decay of the underlying waveform, following
901 minis (MD & GM, unpublished observations). Alternatively, noise traces can be used to more
902 accurately 'reverse-engineer' the signal distribution via simulations, by iteratively adjusting the
903 shapes, amplitudes, and incidence rates of simulated minis, and adding these to real noise, under
904 the control of an optimisation algorithm to match up the distributions of *simulated* minis plus real
905 noise to *real* minis plus real noise. A companion article explores this and presents a quantal analysis
906 method based on the 'minis' spontaneous postsynaptic event detection algorithm.
907

References

Agmon-Snir H, Segev I. 1993. Signal delay and input synchronization in passive dendritic structures. *J Neurophysiol* **70**:2066–2085. doi:10.1152/jn.1993.70.5.2066

Brown TH, Wong RKS, Prince DA. 1979. Spontaneous miniature synaptic potentials in hippocampal neurons. *Brain Res* **177**:194–199. doi:https://doi.org/10.1016/0006-8993(79)90931-4

Clements JD, Bekkers JM. 1997. Detection of spontaneous synaptic events with an optimally scaled template. *Biophys J* **73**:220–229. doi:https://doi.org/10.1016/S0006-3495(97)78062-7

De Koninck Y, Mody I. 1994. Noise analysis of miniature IPSCs in adult rat brain slices: properties and modulation of synaptic GABAA receptor channels. *J Neurophysiol* **71**:1318–1335. doi:10.1152/jn.1994.71.4.1318

del Castillo J, Katz B. 1954. Quantal components of the end-plate potential. *J Physiol* **124**:560–573. doi:https://doi.org/10.1113/jphysiol.1954.sp005129

Dervinis M. 2022. minis. *https://github.com/dervinism/minis*. https://github.com/dervinism/minis

El Khoueiry C, Alba-Delgado C, Antri M, Gutierrez-Mecinas M, Todd AJ, Artola A, Dallel R. 2022. GABAA and Glycine Receptor-Mediated Inhibitory Synaptic Transmission onto Adult Rat Lamina IIi PKCγ-Interneurons: Pharmacological but Not Anatomical Specialization. *Cells* **11**. doi:10.3390/cells11081356

Fatt P, Katz B. 1952. Spontaneous subthreshold activity at motor nerve endings. *J Physiol* **117**:109–128.

Glasgow SD, McPhedrain R, Madranges JF, Kennedy TE, Ruthazer ES. 2019. Approaches and Limitations in the Investigation of Synaptic Transmission and Plasticity. *Front Synaptic Neurosci* **11**. doi:10.3389/fnsyn.2019.00020

Hwang TN, Copenhagen DR. 1999. Automatic detection, characterization, and discrimination of kinetically distinct spontaneous synaptic events. *J Neurosci Methods* **92**:65–73. doi:https://doi.org/10.1016/S0165-0270(99)00095-3

Isaac JTR, Nicoll RA, Malenka RC. 1995. Evidence for silent synapses: Implications for the expression of LTP. *Neuron* **15**:427–434. doi:https://doi.org/10.1016/0896-6273(95)90046-2

Isaacson JS, Walmsley B. 1995. Counting quanta: Direct measurements of transmitter release at a central synapse. *Neuron* **15**:875–884. doi:10.1016/0896-6273(95)90178-7

Larkum ME, Nevian T, Sandler M, Polsky A, Schiller J. 2009. Synaptic Integration in Tuft Dendrites of Layer 5 Pyramidal Neurons: A New Unifying Principle. *Science (1979)* **325**:756–760. doi:10.1126/science.1171958

Liao D, Hessler NA, Malinow R. 1995. Activation of postsynaptically silent synapses during pairing-induced LTP in CA1 region of hippocampal slice. *Nature* **375**:400–404. doi:10.1038/375400a0

Liao D, Jones A, Malinow R. 1992. Direct measurement of quantal changes underlying long-term potentiation in CA1 hippocampus. *Neuron* **9**:1089–1097. doi:https://doi.org/10.1016/0896-6273(92)90068-O

Macmillan NA, Creelman CD. 2005. Detection theory: A user's guide, 2nd ed., Detection theory: A user's guide, 2nd ed. Mahwah, NJ, US: Lawrence Erlbaum Associates Publishers.

Major G, Evans JD, Jack JJ. 1993. Solutions for transients in arbitrarily branching cables: I. Voltage recording with a somatic shunt. *Biophys J* **65**:423–449. doi:10.1016/S0006-3495(93)81037-3

Major G, Larkman AU, Jonas P, Sakmann B, Jack JJ. 1994. Detailed passive cable models of whole-cell recorded CA3 pyramidal neurons in rat hippocampal slices. *The Journal of Neuroscience* **14**:4613. doi:10.1523/JNEUROSCI.14-08-04613.1994

Major G, Larkum ME, Schiller J. 2013. Active Properties of Neocortical Pyramidal Neuron Dendrites. *Annu Rev Neurosci* **36**:1–24. doi:10.1146/annurev-neuro-062111-150343

Nevian T, Larkum ME, Polsky A, Schiller J. 2007. Properties of basal dendrites of layer 5 pyramidal neurons: a direct patch-clamp recording study. *Nat Neurosci* **10**:206–214. doi:10.1038/nn1826

Rall W. 1977. Core Conductor Theory and Cable Properties of Neurons In: Kandel ER, Brookhardt JM, Mountcastle VM, editors. Handbook of Physiology, Cellular Biology of Neurons. Bethesda, MD: American Physiological Society. pp. 39–97.

Rall W. 1967. Distinguishing theoretical synaptic potentials computed for different soma-dendritic distributions of synaptic input. *J Neurophysiol* **30**:1138–1168. doi:10.1152/jn.1967.30.5.1138

Rinzel J, Rall W. 1974. Transient Response in a Dendritic Neuron Model for Current Injected at One Branch. *Biophys J* **14**:759–790. doi:https://doi.org/10.1016/S0006-3495(74)85948-5

Sara Y, Bal M, Adachi M, Monteggia LM, Kavalali ET. 2011. Use-Dependent AMPA Receptor Block Reveals Segregation of Spontaneous and Evoked Glutamatergic Neurotransmission. *The Journal of Neuroscience* **31**:5378. doi:10.1523/JNEUROSCI.5234-10.2011

Segal M. 2010. Dendritic spines, synaptic plasticity and neuronal survival: activity shapes dendritic spines to enhance neuronal viability. *European Journal of Neuroscience* **31**:2178–2184. doi:https://doi.org/10.1111/j.1460-9568.2010.07270.x

Shi Y, Nenadic Z, Xu X. 2010. Novel Use of Matched Filtering for Synaptic Event Detection and Extraction. *PLoS One* **5**:e15517-.

Stuart G, Spruston N. 1998. Determinants of Voltage Attenuation in Neocortical Pyramidal Neuron Dendrites. *The Journal of Neuroscience* **18**:3501–3510. doi:10.1523/JNEUROSCI.18-10-03501.1998

Wall MJ, Usowicz MM. 1998. Development of the quantal properties of evoked and spontaneous synaptic currents at a brain synapse. *Nat Neurosci* **1**:675–682. doi:10.1038/3677

Williams SR, Mitchell SJ. 2008. Direct measurement of somatic voltage clamp errors in central neurons. *Nat Neurosci* **11**:790–798. doi:10.1038/nn.2137

Williams SR, Stuart GJ. 2002. Dependence of EPSP Efficacy on Synapse Location in Neocortical Pyramidal Neurons. *Science (1979)* **295**:1907–1910. doi:10.1126/science.1067903

Figures

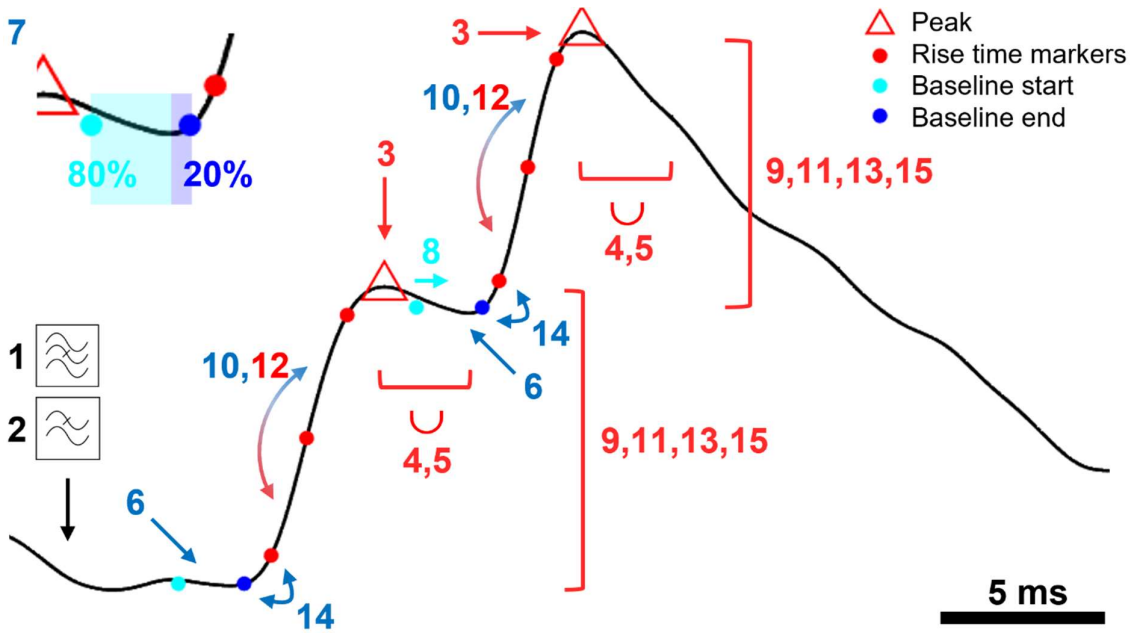

Figure 1: A Schematic representation of key steps in 'minis' detection algorithm.

An illustration of a step-by-step application of the mPSP/C detection algorithm using simulated data. Numbered steps dealing with mini peaks/amplitudes are shown in red, steps used to determine the baseline are shown in blue. Briefly, the steps are:

1. Bandstop filter (against mains).
2. Lowpass filter to remove high frequency noise.
3. Find peaks.
4. Discard smaller peaks with the peak integration period represented by the length of the bracket and the union symbol (∪).
5. Move to a higher peak (if exists) within the peak integration period discarding the earlier peak.
6. Position the baseline at a local minimum located within the time-to-peak period prior to the peak.

7. Position the baseline asymmetrically (80:20) around the minimum (colour change at the inset).
8. Correct the start of the baseline if it overlaps with the previous peak.
9. Discard the peak if it falls outside the acceptable amplitude range (repeated three more times).
10. Compare rise time halves to correct the baseline (can be repeated once more).
11. Repeat Step 9.
12. Compare rise time halves to correct the peak.
13. Repeat Step 9.
14. Correct the baseline if it significantly deviates from the 10%/20% rise time mark.
15. Repeat Step 9.

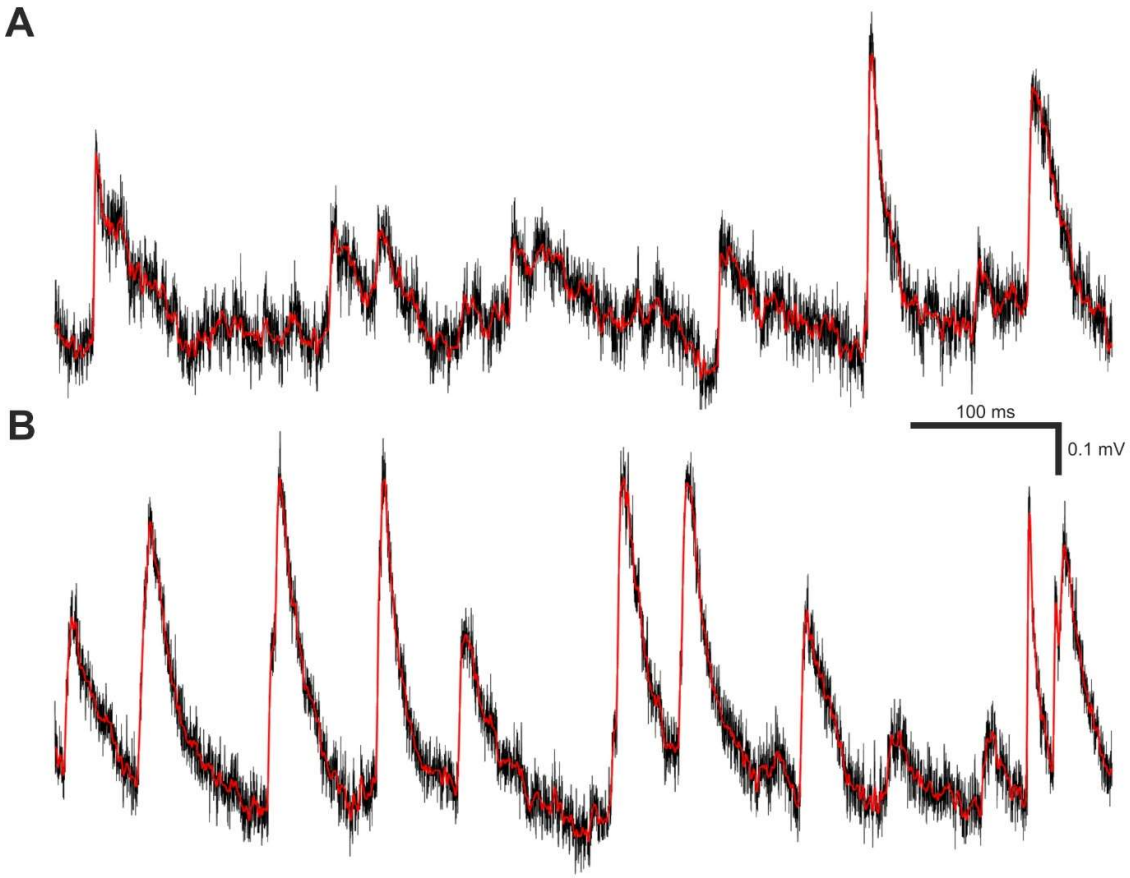

Figure 2: Filtering and smoothing effects.

(A) A brief segment of V_m trace recording containing real minis and noise. The black trace is raw (unfiltered and unsmoothed), whereas the red trace is the same data after filtering and smoothing as described in Materials and Methods subsection called *'minis' detection algorithm*.

(B) Same as (A) but containing varying amplitude smEPSPs with a 20 minis/s incidence rate instead of real minis.

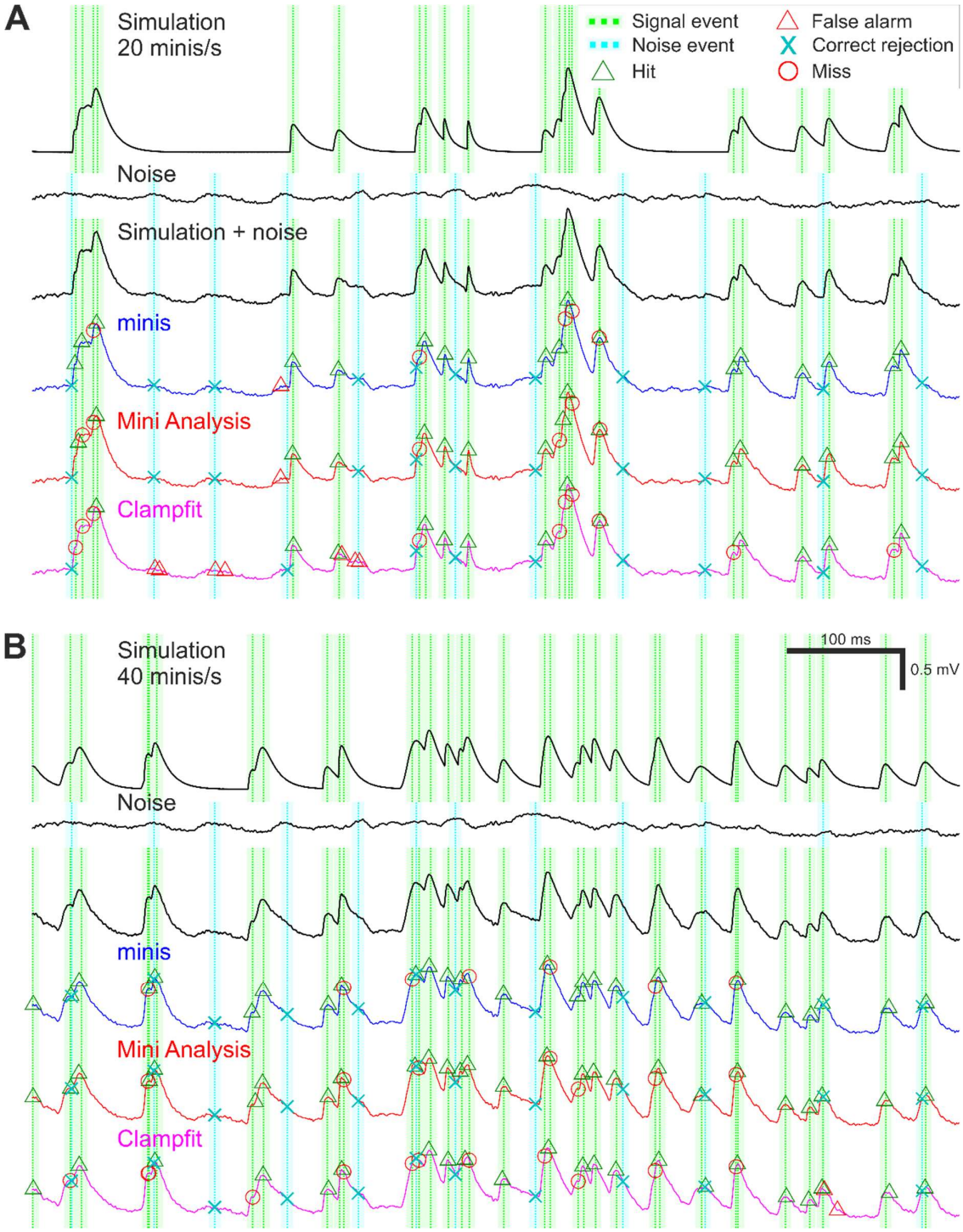

Figure 2: Simulation and detection performance.

(A) An example of simulated membrane potential recording with average simulated mEPSP incidence rate of 20 minis/s. The top voltage trace shows a brief segment with randomly timed smEPSPs with random, normally-distributed amplitudes (μ_1= 0.3 mV, σ_1 = 0.05 mV) and 10-90% rise

1021 times (drawn from the upper half of the distribution with μ_2 = 0.05 ms, σ_2 = 2.5 ms); see Methods.

1022 Dotted green vertical lines mark signal events corresponding to smEPSP peaks. The paler shaded

1023 colour demarcates a 10-ms (± 5 ms) window for accepting the detection of a signal event. The

1024 second traces from the top are corresponding recordings of V_m noise fluctuations (the 2nd recording

1025 phase: 'noise-alone' condition, in TTX and transmitter blockers), after initial filtering and smoothing

1026 (steps 1 and 2 of the 'minis' detection algorithm; Figure 2). Dotted vertical cyan lines indicate noise

1027 events; the shaded colour demarcates a window of exclusion for correctly rejecting these events

1028 (see Methods). The V_m third from the top trace is a hybrid one with smEPSPs added to the noise

1029 recording and with signal events and noise 'events' indicated. The coloured V_m traces below show

1030 detection performance for the three different algorithms.

1031 (B) An example of simulated V_m recording with mEPSP incidence rate of 40 minis/s.

1032

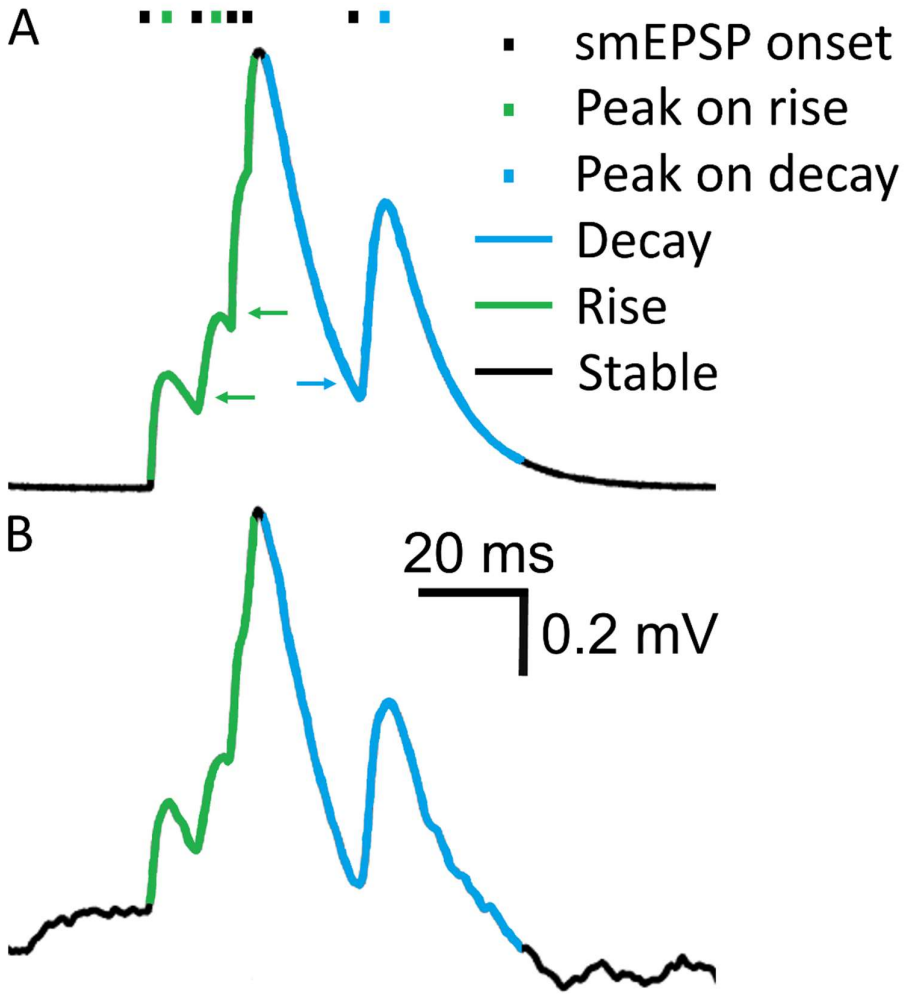

Figure 3: Membrane potential rising, steady-ish and falling 'trend phases'.

(A) A short segment of a V_m trace showing five smEPSPs. Different V_m 'trend phases', based on the overall upward or downward trend in *simulated* voltage, are marked in colour. Green arrows indicate V_m points where the V_m rate of increase is assigned to the preceding mEPSP peak. The blue arrow indicates a V_m point where the V_m rate of decay is assigned to the following mEPSP peak. (B) Simulated V_m trace in (A) added to a noise recording. V_m 'trend phases' were determined in (A) and are used to classify detected events in (B).

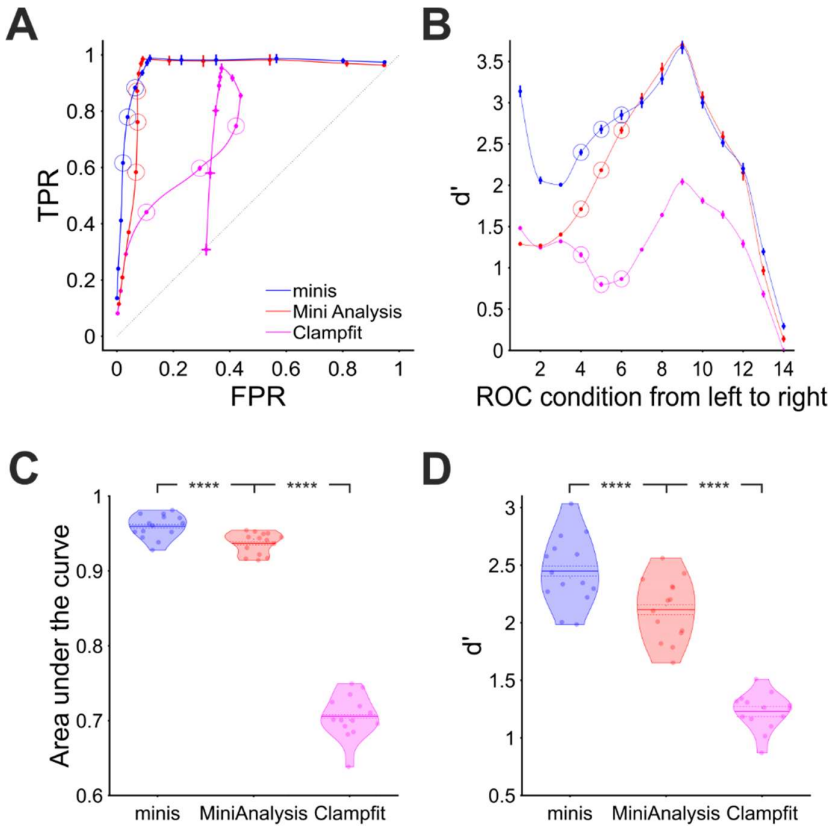

Figure 4: Overall performance for detecting 'moderately'-sized smEPSPs (~0.3 mV). (A) 'virtual' ROC (Receiver Operator Characteristic)-like curve showing performance for detecting 'moderately'-sized smEPSPs in terms of True Positive Rate TPR (sensitivity) and False Positive Rate FPR (1 – specificity) for all three algorithms, averaged across all 14 cells. In each case, dataset varies from point to point, as opposed to detection threshold itself (which is varied systematically in a traditional ROC, using one dataset). Ideal performance would be a right-angle plot going vertically up TPR-axis at FPR=0, then horizontally along the top of the plot at TPR=1; minis is close to ideal, and superior to MiniAnalysis, which is not too far from ideal (despite its 'missed minis' problems). Clampfit is far from ideal. Different points represent 14 different incidence rate/signal-to-noise ratio conditions, averaged across all 14 cells. Moving (generally) from bottom to top/left to right, simulated minis rates and signal-to-noise ratio are decreasing. Vertical and horizontal bars indicate 95% confidence interval around each mean. The dotted diagonal line indicates chance performance. The hollow circles mark three realistic smEPSP incidence rates (80, 40, and 20 minis/s).

1056 (B) Sensitivity (discriminability) index (d') in the same 14 conditions as in (A) for all three algorithms,
1057 averaged across all 14 cells.
1058 (C) 'Violin' plots for Area under the virtual-ROC curve in (A) for all three algorithms. Individual data
1059 points represent the 14 individual recordings (cells), horizontally 'swarmed' to avoid overlaps. AUC
1060 (Area Under Curve) is averaged across all 14 incidence rate/signal-to-noise conditions for each cell
1061 for each detection algorithm. The mean is marked by a solid line over the 'violin' centre. The dashed
1062 line indicates the 95% confidence limits of the mean, and coloured shapes indicate the approximate
1063 (smoothed) probability densities (wider = higher probability of those values).
1064 **** indicates (highly) significantly different at $p \leq 10^{-5}$ level, paired t-test.
1065 (D) Similar plot for sensitivity index d' averaged across all 14 incidence rate/signal-to-noise
1066 conditions for each cell and each detection algorithm.
1067

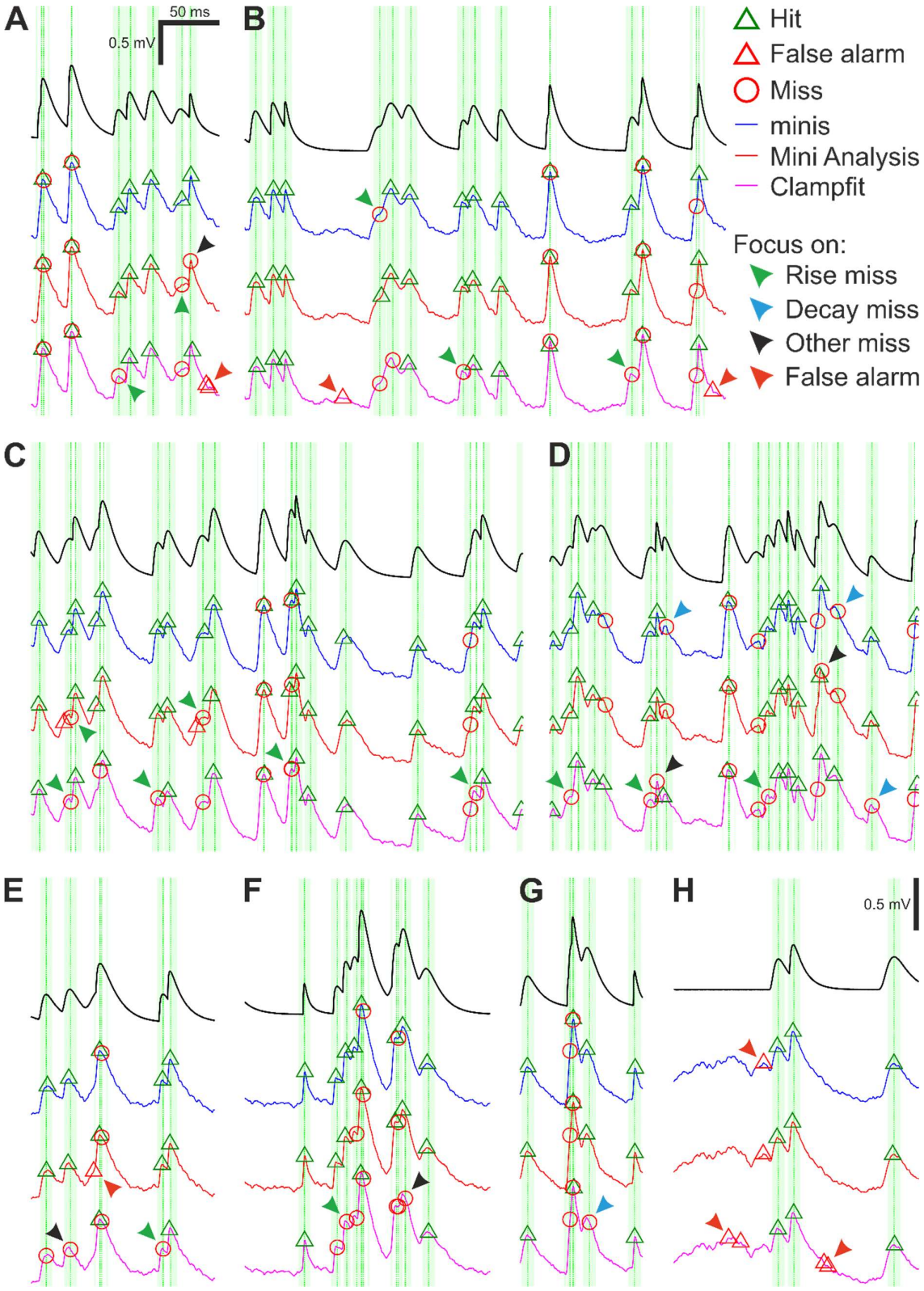

Figure 5: Moderately-sized (~0.3 mV) smEPSPs (40 minis/s): detection errors made by the three algorithms.

1071 (A-H) Examples of smEPSP detection errors commonly committed by the three algorithms. Traces in
1072 blue, red, and magenta represent detection performance for 'minis', MiniAnalysis, and Clampfit,
1073 respectively. The top black trace shows actual smEPSPs. Vertical green dotted lines mark actual
1074 individual (i.e., non-summated) smEPSP peak locations with the fainter shaded colour demarcating a
1075 10-ms window for accepting the detection of an mEPSP. Arrowheads indicate common detection
1076 errors made by the three algorithms. (Details in text).
1077

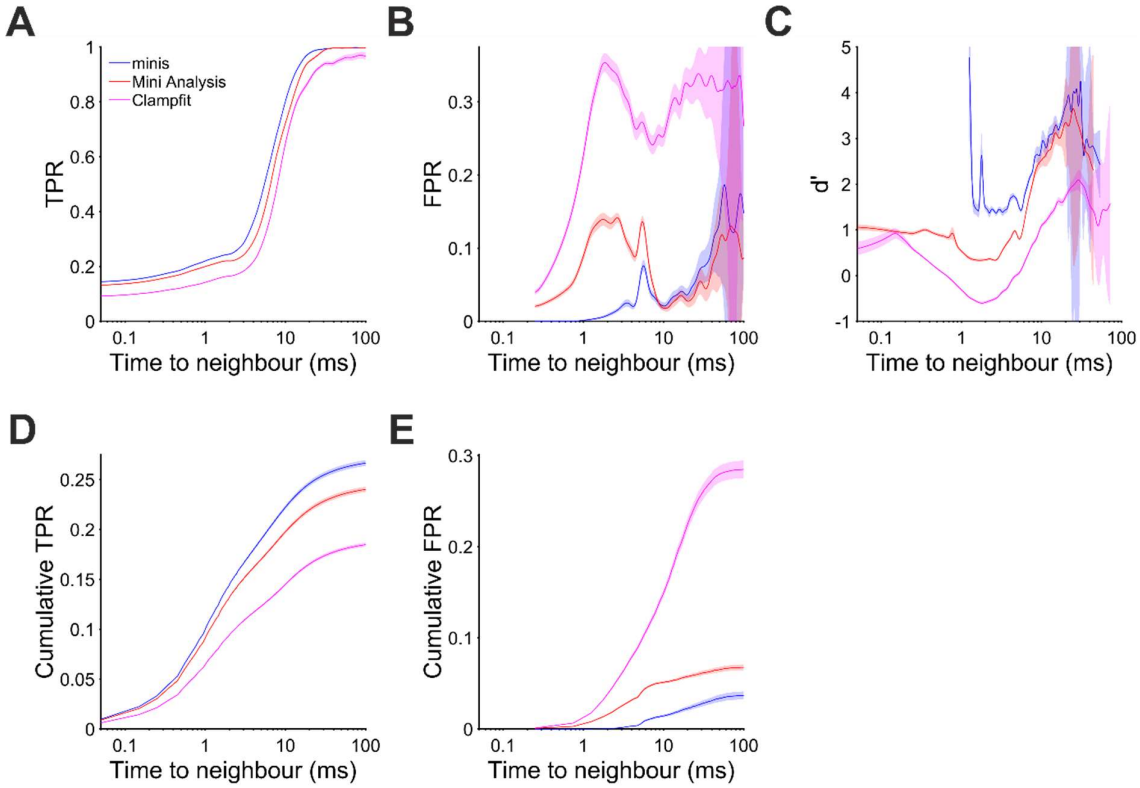

Figure 6: Performance when detecting moderately-sized (~0.3 mV) smEPSPs as a function of time to the nearest neighbour (mean inter-mini peak-to-peak interval). Pale shaded colours indicate 95% confidence intervals.

(A) True positive rate (TPR).

(B) False positive rate (FPR).

(C) Sensitivity index d' (undefined but arbitrarily high for TPR > 0 and FPR = 0, e.g. for inter-mini intervals below 1 ms, for minis algorithm).

(D) Cumulative true positive rate (TPR) (cumulative true positives normalised by the total unbanded true positive count and scaled by the overall unbanded TPR; see text for details).

(E) Cumulative FPR (cumulative false positives normalised by the total unbanded false positive count and scaled by the overall unbanded FPR).

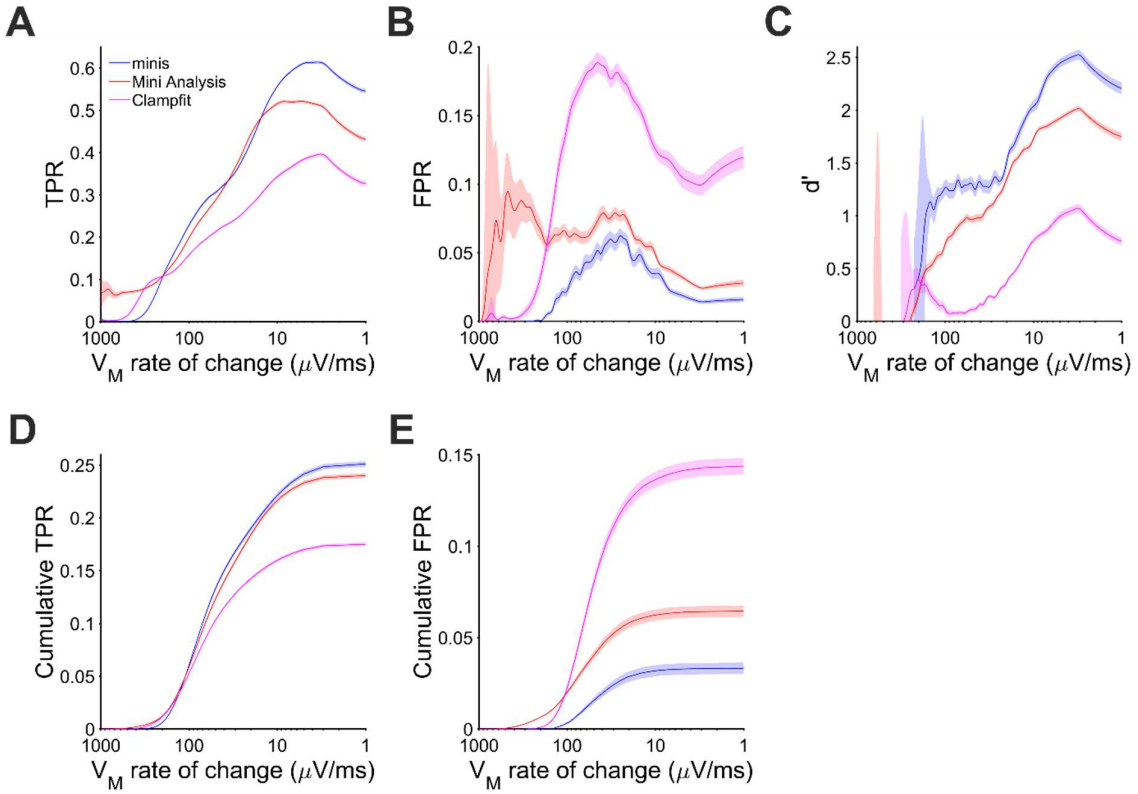

Figure 7: Performance when detecting moderately-sized (~0.3 mV) smEPSPs on a rising trend V_m as a function of the V_m rate of change. Paler shaded colours indicate 95% confidence intervals.

(A) True positive rate (TPR).

(B) False positive rate (FPR).

(C) Sensitivity index d'.

(D) Cumulative TPR.

(E) Cumulative FPR.

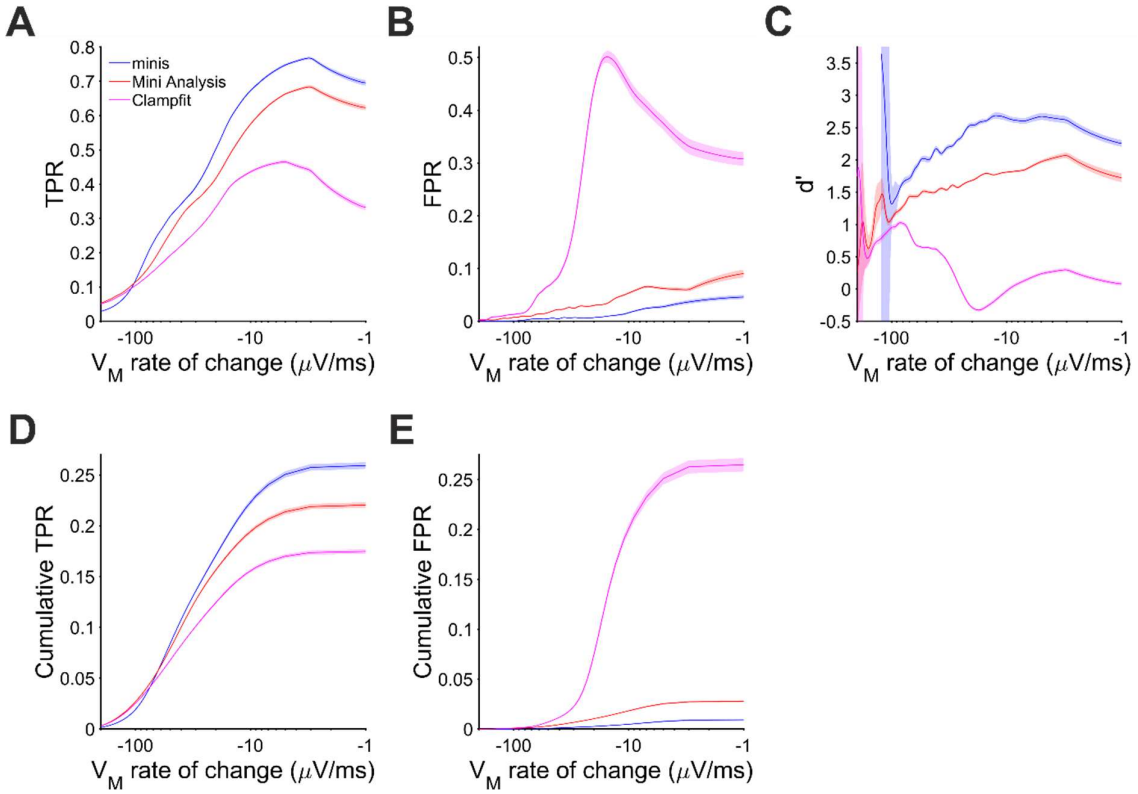

Figure 8: Performance when detecting moderately-sized (~0.3 mV) smEPSPs on the membrane potential decaying trend phase as a function of the membrane potential rate of change. Paler shaded colours indicate 95% confidence intervals.

(A) True positive rate (TPR)

(B) False positive rate (FPR).

(C) Sensitivity Index d'.

(D) Cumulative TPR.

(E) Cumulative FPR.

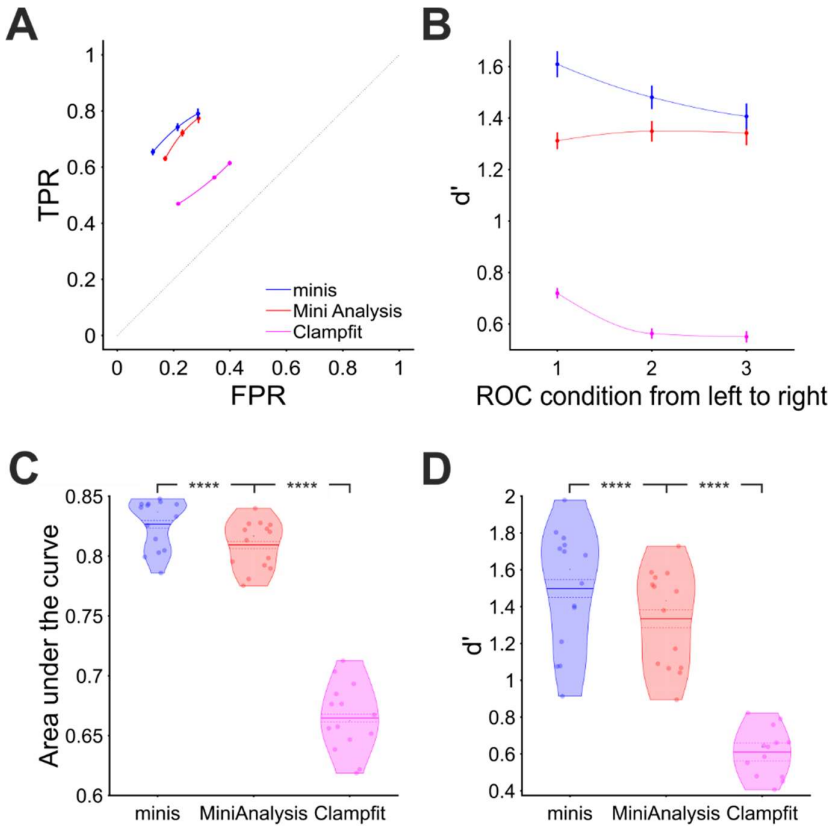

Figure 12: Overall performance for detecting smEPSPs of various (realistic) discrete amplitudes at 'realistic' minis' rates (details in text).

(A) Partial virtual "ROC" curve showing performance for detecting small-to-large-sized smEPSPs (0.05 to 0.5 mV in increments of 0.05 mV selected and added at random to a noise trace from each of the 14 cells) in terms of TPR (sensitivity) and FPR (1 – specificity) for all three algorithms. Moving from left to right different data points represent 3 different biologically realistic incidence rate conditions: 61, 38, and 27 minis/s. Vertical and horizontal bars indicate 95% confidence interval around the mean. The dotted diagonal line indicates chance performance.

(B) Sensitivity index (d') when detecting smEPSPs in the same 3 conditions as in (A) for all three algorithms.

(C) Area under the virtual-ROC curve in (A) for all three algorithms. Individual data points represent individual recordings (n=14 cells), averaged over the three simulated minis incidence rates. The

1123 mean is marked by a solid line over the violin centre. The dashed line indicates the 95% confidence

1124 limits. **** indicates (highly) significantly different at $p \leq 10^{-5}$ level, paired t-test.

1125 (D) Sensitivity index d' averaged across all three simulated minis incidence rates, for each cell (n=14),

1126 separately for each detection algorithm.

1127

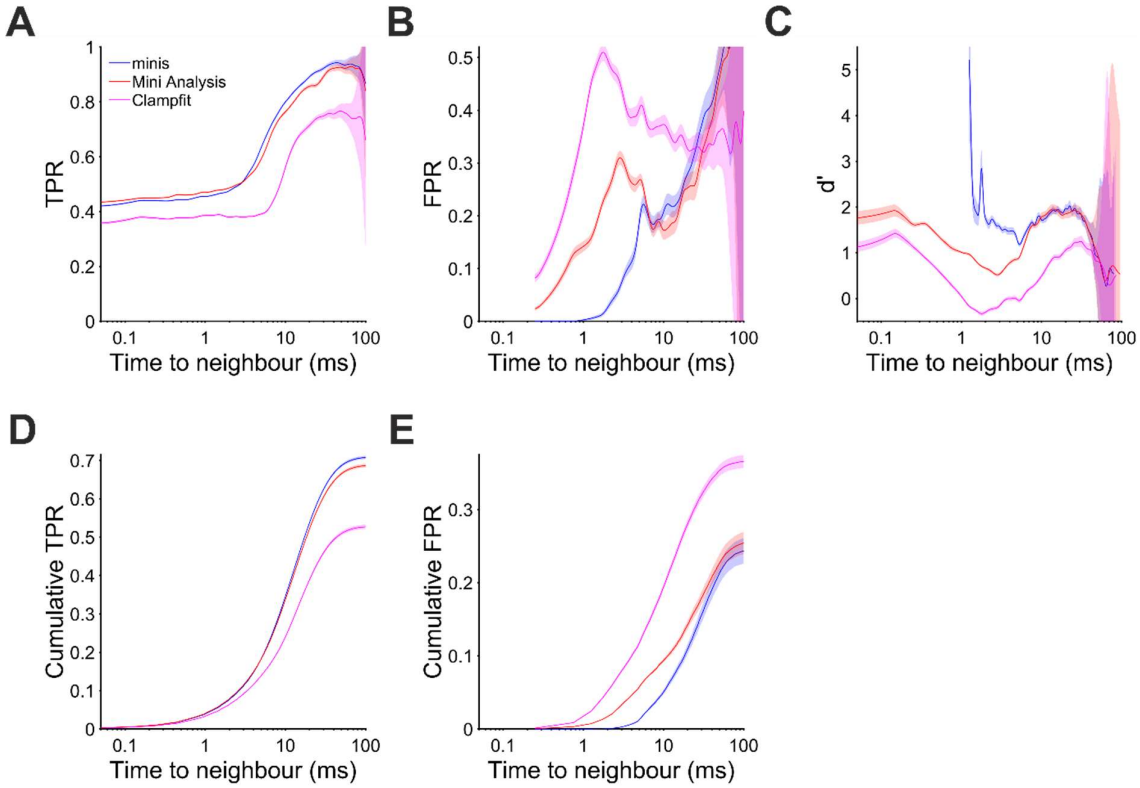

Figure 13: Performance for detecting smEPSPs of various (realistic) discrete amplitudes as a function of the time to the nearest neighbour.

(A) True positive rate (TPR) when detecting smEPSPs of various discrete amplitudes (0.05 to 0.5 mV in increments of 0.05 mV) added at random to noise waveforms, as in previous figure, as a function of the time to the nearest neighbour. Pale shaded colours indicate 95% confidence intervals.

(B) False positive rate (FPR).

(C) d' (undefined but arbitrarily high for TPR > 0 and FPR = 0, e.g. for inter-mini intervals below 1 ms, for minis algorithm).

(D) Cumulative TPR.

(E) Cumulative FPR.

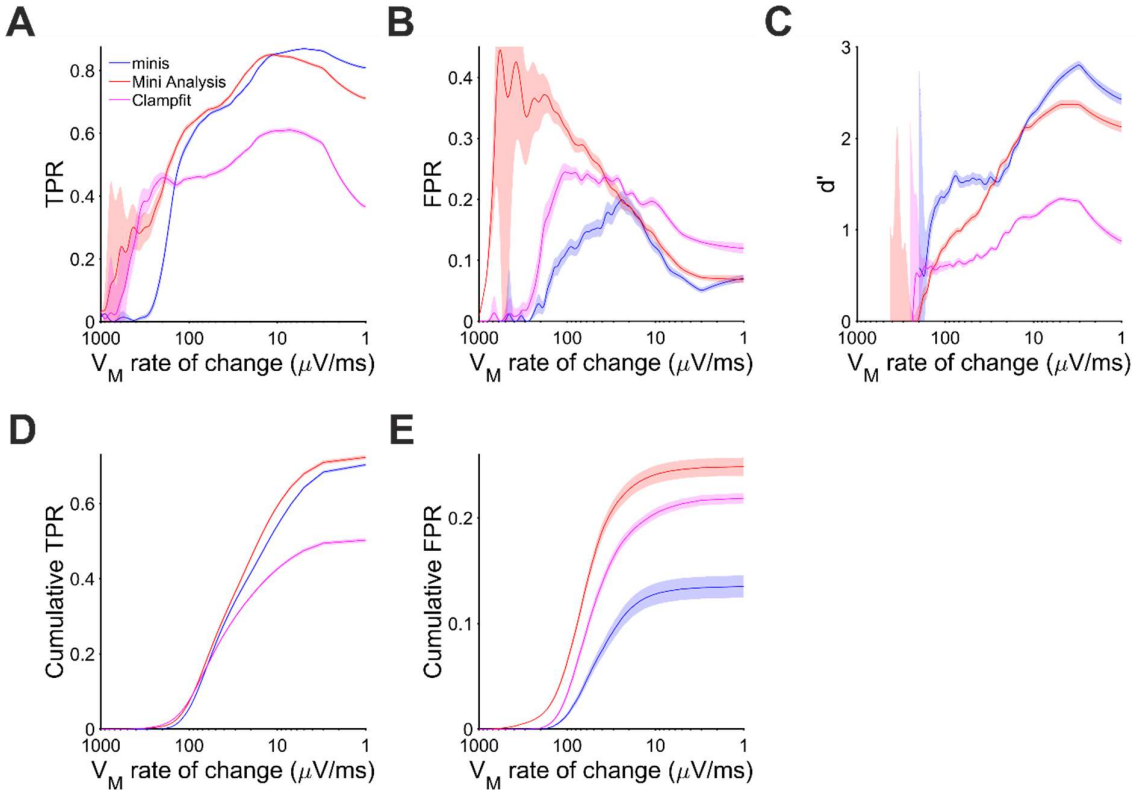

Figure 14: Performance for detecting smEPSPs of (realistic) discrete amplitudes on the membrane potential rise phase.

(A) True positive rate (TPR) when detecting smEPSPs of various amplitudes (0.05 to 0.5 mV in increments of 0.05 mV, added at random to noise waveforms, as in the previous figure), on the V_m rise phase as a function of the V_m rate of change. Pale shaded colours indicate 95% confidence intervals.

(B) False positive rate (FPR).

(C) d'.

(D) Cumulative TPR.

(E) Cumulative FPR.

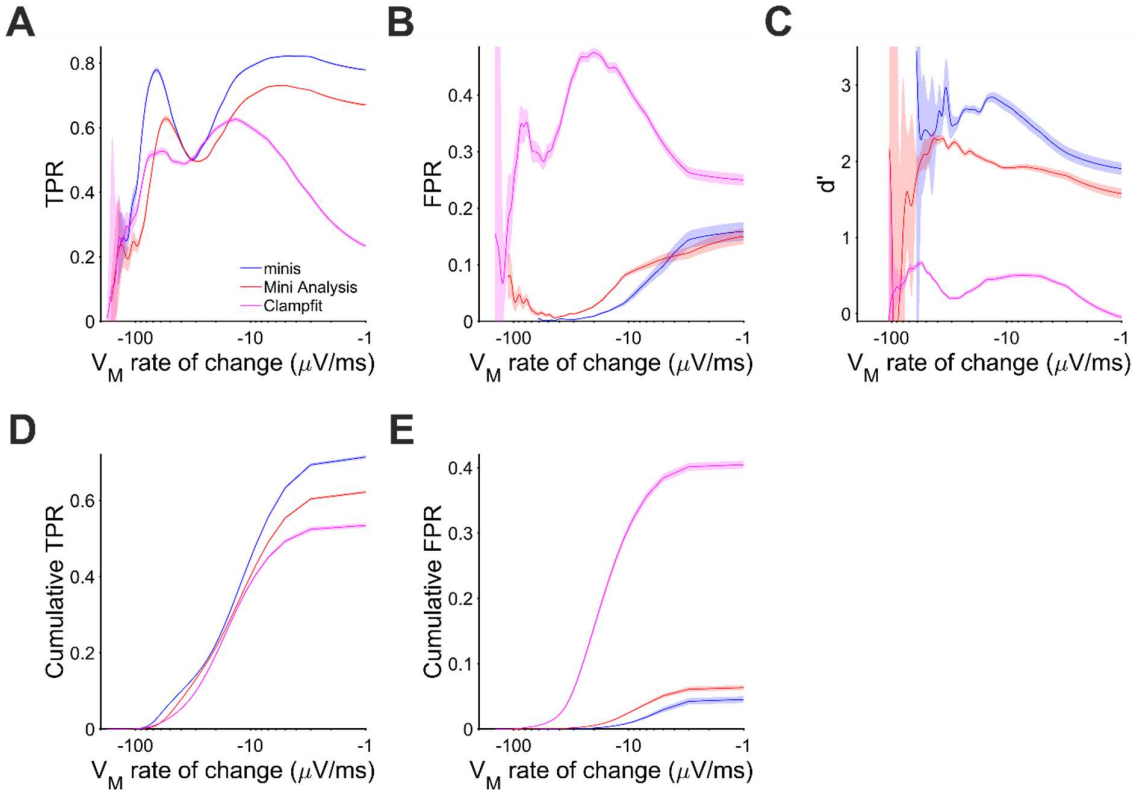

Figure 15: Performance for detecting smEPSPs of (realistic) discrete amplitudes on the membrane potential decay phase under realistic incidence rate conditions.

(A) True positive rate (TPR) when detecting smEPSPs of various amplitudes (0.05 to 0.5 mV in increments of 0.05 mV, as in previous figure) on the V_m decay phase, as a function of the V_m rate of change. Pale shaded colours indicate 95% confidence intervals.

(B) false positive rate (FPR).

(C) d'.

(D) Cumulative TPR.

(E) Cumulative FPR.

Condition	Truth	Minis ± 95% CI	Range	MiniAnalysis ± 95% CI	Range	Clampfit ± 95% CI	Range
Type 1 All	0.3	0.36±0.003	0.1-4.49	0.43±0.003	0.1-5.78	0.45±0.005	0.005-8.32
Type 1 HI	0.3	0.44±0.003	0.1-4.49	0.53±0.002	0.1-4.32	0.49±0.004	0.005-8.32
Type 1 RI	0.3	0.31±0.004	0.1-2.46	0.36±0.004	0.1-2.48	0.35±0.006	0.005-2.73
Type 2	0.275	0.29±0.002	0.06-2.48	0.32±0.002	0.06-2.35	0.34±0.004	0.05-1.2
Real data	-	0.05±0.001	0.02-3.97	0.09±0.002	0.02-4.87	0.21±0.006	0.07-2.67

Table 1: Mean amplitudes of detected simulated and real minis by the three different algorithms. All values are given in mV. Abbreviations: Confidence interval (CI), all conditions with 0.3 mV amplitude simulated minis used to construct the virtual ROC curve (Type 1 All), high incidence rate conditions (640, 320, and 160 minis/s) with 0.3 mV amplitude simulated minis used to construct the virtual ROC curve (Type 1 HI), realistic incidence rate conditions (80, 40, and 20 minis/s) with 0.3 mV amplitude simulated minis used to construct the virtual ROC curve (Type 1 RI), all realistic incidence rate conditions with varying amplitude simulated minis (Type 2).

Condition	Minis vs MiniAnalysis	Minis vs Clampfit	Minis vs truth	MiniAnalysis vs Clampfit	MiniAnalysis vs truth	Clampfit vs truth
Type 1 All	$4.35*10^{-15}$	$8.49*10^{-6}$	$1.01*10^{-7}$	0.22	$3.91*10^{-12}$	$7.49*10^{-10}$
Type 1 HI	$3.27*10^{-18}$	$2.87*10^{-6}$	$3.49*10^{-13}$	$2.94*10^{-5}$	$5.84*10^{-17}$	$1.39*10^{-12}$
Type 1 RI	$3.94*10^{-13}$	0.0057	0.17	0.84	$8.89*10^{-6}$	0.00021
Type 2	$1.14*10^{-12}$	$5.29*10^{-5}$	$1.18*10^{-5}$	0.0066	$7.48*10^{-9}$	$1.26*10^{-7}$
Real data	$1.29*10^{-9}$	$5.05*10^{-10}$	-	$1.59*10^{-8}$	-	-

Table 2: T-test p-values for mean amplitude values of detected minis using different algorithms. Repeated measures t-tests were used when comparing performance of two algorithms and single sample t-tests were used when comparing mean values with ground truth (subtracting ground truth values). Abbreviations are the same as in Table 1.

Condition	Truth	Minis ± 95% CI	Range	MiniAnalysis ± 95% CI	Range	Clampfit ± 95% CI	Range
Type 1 All	2.6	3.31±0.018	0.55-9.15	3.7±0.015	0.01-22.3	5.05±0.022	0.05-39.4
Type 1 HI	2.6	3.05±0.005	0.55-8.8	3.37±0.004	0.01-20.8	5.12±0.018	0.05-39.4
Type 1 RI	2.6	3.97±0.037	0.75-9.1	3.9±0.041	0.01-22.3	4.8±0.032	0.05-39.4
Type 2	2.6	3.69±0.014	0.65-9	3.29±0.022	0.02-57.5	4.77±0.013	0.06-35.9
Real data	-	3.37±0.044	0.35-9.4	3.42±0.051	0.02-18	4.72±0.052	0.09-37

Table 3: Mean 10-90% rise times of detected simulated and real minis by the three different **algorithms.** All values are given in ms. Abbreviations are the same as in Table 1.

Condition	Minis vs MiniAnalysis	Minis vs Clampfit	Minis vs truth	MiniAnalysis vs Clampfit	MiniAnalysis vs truth	Clampfit vs truth
Type 1 All	$9.94*10^{-13}$	$1.14*10^{-14}$	$1.33*10^{-11}$	$1.12*10^{-14}$	$5.03*10^{-15}$	$1.54*10^{-17}$
Type 1 HI	$5.61*10^{-15}$	$3.54*10^{-18}$	$4.68*10^{-16}$	$1.13*10^{-17}$	$4.33*10^{-21}$	$9.95*10^{-19}$
Type 1 RI	$6.08*10^{-08}$	$2.21*10^{-12}$	$4.14*10^{-10}$	$6.47*10^{-11}$	$2.16*10^{-10}$	$5.47*10^{-15}$
Type 2	0.0024	$1.46*10^{-17}$	$1.31*10^{-13}$	$3.49*10^{-16}$	$2.13*10^{-10}$	$5.98*10^{-20}$
Real data	$8.61*10^{-15}$	$4.83*10^{-13}$	-	$2.82*10^{-08}$	-	-

Table 4: T-test p-values for mean 10-90% rise time values of detected minis using different **algorithms.** Repeated measures t-tests were used when comparing performance of two algorithms and single sample t-tests were used when comparing mean values with ground truth. Abbreviations are the same as in Table 1.

Condition	Truth ± 95% CI	Minis ± 95% CI	Range	MiniAnalysis ± 95% CI	Range	Clampfit ± 95% CI	Range
Type 1 All	10.9±0.33	11.2±0.22	0.65-30.1	13.2±0.1	0.05-30.1	7.75±0.03	0.18-30.1
Type 1 HI	10.9±0.33	9.8±0.16	0.65-30.1	12.7±0.078	0.05-30.1	7.73±0.02	0.18-30.1
Type 1 RI	10.9±0.33	10.9±0.19	0.8-30.1	14.1±0.14	0.05-30.1	7.63±0.05	0.2-29.7
Type 2	10.9±0.33	10.9±0.19	0.75-30.1	13.9±0.13	0.05-30.1	7.37±0.04	0.16-28.2
Real data	-	11.2±0.44	0.45-30.1	12.3±0.24	0.05-30.1	7.02±0.06	0.28-28.9

Table 5: Mean decay times of detected simulated and real minis by the three different algorithms. All values are given in ms. Abbreviations are the same as in Table 1.

Condition	Minis vs MiniAnalysis	Minis vs Clampfit	Minis vs truth	MiniAnalysis vs Clampfit	MiniAnalysis vs truth	Clampfit vs truth
Type 1 All	$1.23*10^{-5}$	$8.43*10^{-7}$	0.3	$1.82*10^{-13}$	0.0006	0.0002
Type 1 HI	$1.1*10^{-10}$	$7.46*10^{-6}$	0.006	$1.07*10^{-13}$	0.002	0.0002
Type 1 RI	$6.84*10^{-10}$	$5.12*10^{-7}$	0.91	$3.78*10^{-12}$	$1.07*10^{-5}$	0.0002
Type 2	$1.71*10^{-11}$	$1.39*10^{-7}$	0.97	$6.87*10^{-13}$	$3.02*10^{-6}$	$6.61*10^{-5}$
Real data	0.17	$1.27*10^{-5}$	-	$3.73*10^{-9}$	-	-

Table 6: T-test p-values for mean decay time values of detected minis using different algorithms. Repeated measures t-tests were used when comparing mean values. Abbreviations are the same as in Table 1.

Condition	Truth	Minis ± 95% CI	Range	MiniAnalysis ± 95% CI	Range	Clampfit ± 95% CI	Range
Type 1 All	93.6	40.8±4.54	29.3-146.5	34.7±0.43	30.4-41.8	12.3±0.13	10.5-13.9
Type 1 HI	379.2	64.1±6.04	41-205.1	53.9±0.3	48.5-55.5	21.5±0.1	20.4-22.4

Type 1 RI	47.4	50±6.85	32.9-209.4	39±0.81	33.2-52.3	20.2±0.39	15.9-24.4
Type 2	39	40.1±5.66	28.5-172.9	32.7±0.41	29.9-37.5	17.9±0.08	17-18.8
Real data	-	94.7±2.67	63.1-124.5	74.3±1.38	55.7-89.7	8.19±0.34	4.34-12.4

Table 7: Mean incidence rates of detected simulated and real minis by the three different algorithms. All values are given in minis/s. Abbreviations are the same as in Table 1.

Condition	Minis vs MiniAnalysis	Minis vs Clampfit	Minis vs truth	MiniAnalysis vs Clampfit	MiniAnalysis vs truth	Clampfit vs truth
Type 1 All	0.471	0.004	$2.09*10^{-5}$	$1.57*10^{-12}$	$1.4*10^{-18}$	$3.93*10^{-27}$
Type 1 HI	0.384	0.002	$3.31*10^{-13}$	$1.99*10^{-18}$	$2.64*10^{-30}$	$3.6*10^{-37}$
Type 1 RI	0.377	0.028	0.835	$3.08*10^{-8}$	$6.6*10^{-5}$	$6.7*10^{-15}$
Type 2	0.417	0.041	0.852	$4.73*10^{-11}$	$1.12*10^{-6}$	$4.96*10^{-22}$
Real data	$2.53*10^{-8}$	$3.4*10^{-11}$	-	$3.4*10^{-11}$	-	-

Table 8. T-test p-values for mean incidence rates values of detected minis using different algorithms. Repeated measures t-tests were used when comparing performance of two algorithms and single sample t-tests were used when comparing mean values with ground truth. Abbreviations are the same as in Table 1.

Supplementary Results

Research literature measuring minis in the central nervous system: Extended report

There were 107 studies in total that matched our criteria. All of these studies used voltage clamp as the electrophysiological method for recording spontaneous and miniature postsynaptic events. We surveyed the software they used to detect these events. The biggest group, ~48%, reported using MiniAnalysis. 26% reported using Clampfit, while 13% used a custom algorithm. The remaining 13% did not specify. We compared the performance of the two most popular detection algorithms, MiniAnalysis and Clampfit, both commercially available, with our new algorithm 'minis'.

35 studies (ca. 32%) reported using a current amplitude detection threshold of which 19 studies specified actual numeric value used (-6.8 ± s.d. 0.44 pA, range of -3 to -20 pA). It is likely that a higher fraction of studies made use of amplitude thresholds as only two explicitly reported not using any detection thresholds. Most of the studies did not give enough details (65% of all studies) to judge one way or the other. However, studies that used MiniAnalysis for detection must have used a detection threshold, as this software requires it.

Out of all the studies, 18 carried out research in neocortical pyramidal cells looking at mPSCs only (spontaneous PSCs excluded). 12 studies reported a mean mEPSC amplitude value of -11.74 ± s.d. 0.77 pA (range of -6.0 to -20.9 pA). 13 studies reported a mean incidence rate value of 3.6 ± s.d. 0.34 per second (range of 1.0 to 8.0 per second).

The total putative excitatory synapse count on a single cortical pyramidal cell can number in the tens of thousands (Eyal et al., 2018b). Layer 2/3 pyramidal cells in rats are thought to have 5,000 to 30,000 putative excitatory synapses (Larkman, 1991; Eyal et al., 2018b). Large-thick-trunk/tufted layer 5 pyramidal cells would have an even larger number of contacts (Larkman, 1991). Therefore, we can roughly assume that for most cortical pyramidal cells the number of putative excitatory

1225 synapses ranges between 5,000 and 50,000. Conservatively, we could assume that only a minority,
1226 roughly 40%, of them are functional ('non-silent') synapses with active zones and post-synaptic
1227 densities containing AMPA receptors (Holler et al., 2021; Motta et al., 2019). Given that a
1228 spontaneous vesicle release at a single release site has been estimated to occur with an approximate
1229 incidence rate of 0.0021 per second (Murthy and Stevens, 1999) and given that there may be at least
1230 2.7 release sites per cortical synapse (Holler et al., 2021), the lower bound incidence rate estimate of
1231 such events within a single cortical pyramidal neuron might be expected to range somewhere
1232 between ca. 10 minis/s and 100 minis/s (5,000*0.4*0.0021*2.7– 50,000*0.4*0.0021*2.7). Incidence
1233 rates values reported in the recent literature are below this predicted range by an order of
1234 magnitude, suggesting a significant fraction of smaller minis may commonly be 'missed' under some
1235 recording conditions. This problem has been observed directly (Nevian et al., 2007), using paired
1236 dendritic and somatic whole-cell patch recordings, albeit using voltage recording rather than voltage
1237 clamp, recording from large layer 5 neocortical pyramidal neurons.
1238
1239 **Detection under realistic incidence rate conditions (20, 40, 80 minis/s)**
1240 Data points used to construct the full v-ROC curve include incidence rate and noise conditions that
1241 were not necessarily realistic. Based on our calculations, the range of mEPSP incidence rates one
1242 might commonly expect during real recordings from neocortical pyramidal neurons is likely to be
1243 between 10 and 100 minis/s (see above; also G.M., unpublished experimental observations); In
1244 Figures 4A and B, 20, 40 and 80 minis/s (from right to left) are highlighted by open circles. Just as
1245 across the entire ROC curve, the performance of 'minis' was superior in this incidence rate range
1246 compared to the other two algorithms with MiniAnalysis coming second, and Clampfit being worst,
1247 by a substantial margin.
1248
1249 Other measures like true positive and false positive rates as functions of the time to the nearest
1250 neighbour and V_m rate of change during the rise or decay phases pointed to a very similar conclusion

1251 made regarding the full ROC curve. First, we found that 'minis' performed better than other
1252 algorithms at detecting mEPSPs that were within 10 ms of other mEPSPs and that at longer delays
1253 MiniAnalysis performed just as well (Supplementary Figure 1). Meanwhile, Clampfit performed
1254 consistently worst across the range of inter-mini intervals, whether measured by d' (Supplementary
1255 Figure 1C) or true positive and false positive rates (Supplementary Figures 1A, B, D, and E). When it
1256 came to V_m rate of change, 'minis' consistently showed the best performance at detecting smEPSPs
1257 occurring with the background V_m rate of change ranging between -40 and 100 µV/s (Supplementary
1258 Figures 2 and 3). This is the range where the vast majority of simulated events occurred
1259 (Supplementary Figures 2D and 3D). In terms of individual TPR and FPR (Supplementary Figures 2A
1260 and B and 3A and B) and cumulative rates (Supplementary Figures 2D and E and 3D and E), the
1261 conclusions are much the same as those made regarding the full virtual ROC curve. Namely, that
1262 'minis' had the largest TPR and the smallest FPR with an exception being the TPR in relation to rising
1263 background (simulated) membrane potential trends (Supplementary Figures 2A and D), with there
1264 being a range (45-100 µV/s) where MiniAnalysis had a slightly higher TPR, but not overall
1265 performance measured as d' (Supplementary Figure 2C). Similar to conditions used to construct the
1266 full ROC curve, Clampfit showed consistently the worst performance by all measures. The
1267 performance of all three algorithms was better with realistic smEPSP incidence rates (Supplementary
1268 Figures 2C and 3C) than over the full 'virtual' ROC curve (Figures 7C and 8C). In summary, evaluation
1269 of detection of mEPSPs simulated at realistic incidence rates supported conclusions made regarding
1270 detection performance under a much broader range of simulation incidence rates.
1271

Supplementary References

Beyal G, Verhoog MB, Testa-Silva G, Deitcher Y, Benavides-Piccione R, DeFelipe J, de Kock CPJ, Mansvelder HD, Segev I. 2018. Human Cortical Pyramidal Neurons: From Spines to Spikes via Models. *Front Cell Neurosci*.

Holler S, Köstinger G, Martin KAC, Schuhknecht GFP, Stratford KJ. 2021. Structure and function of a neocortical synapse. *Nature* **591**:111–116. doi:10.1038/s41586-020-03134-2

Larkman AU. 1991. Dendritic morphology of pyramidal neurones of the visual cortex of the rat: III. Spine distributions. *Journal of Comparative Neurology* **306**:332–343. doi:https://doi.org/10.1002/cne.903060209

Motta A, Berning M, Boergens KM, Staffler B, Beining M, Loomba S, Hennig P, Wissler H, Helmstaedter M. 2019. Dense connectomic reconstruction in layer 4 of the somatosensory cortex. *Science (1979)* **366**:eaay3134. doi:10.1126/science.aay3134

Murthy VN, Stevens CF. 1999. Reversal of synaptic vesicle docking at central synapses. *Nat Neurosci* **2**:503–507. doi:10.1038/9149

Supplementary Figures

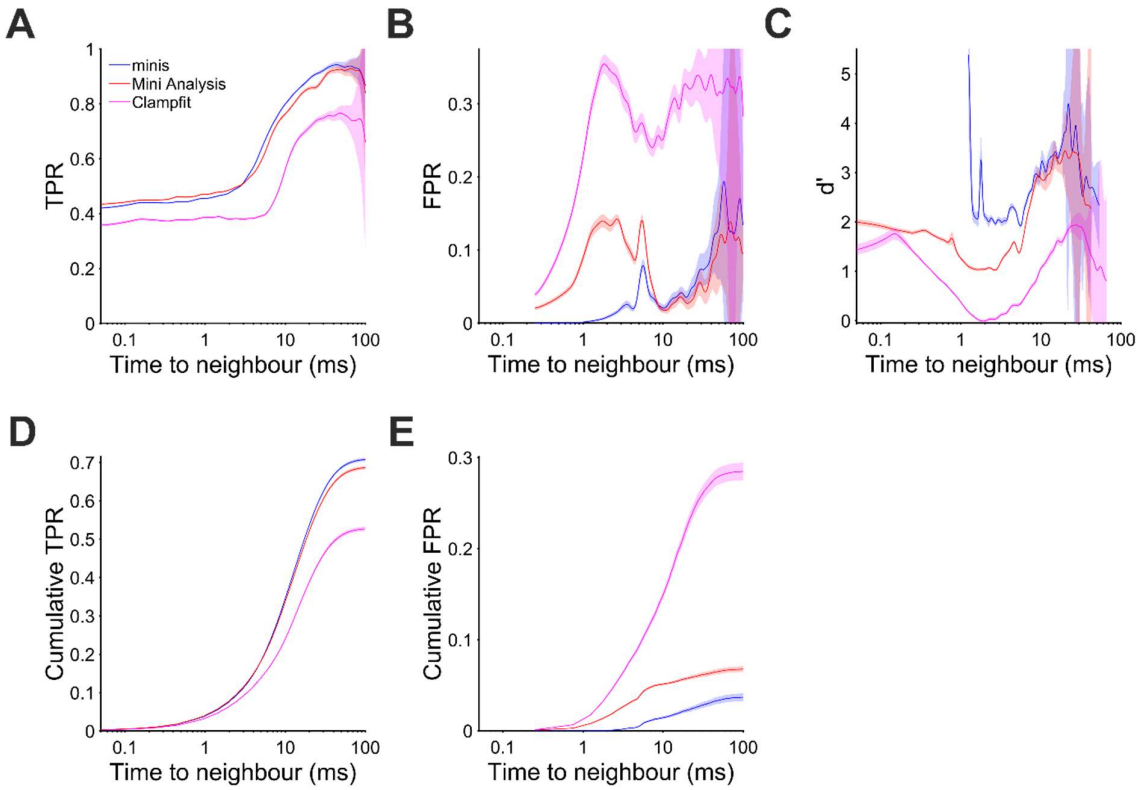

Supplementary Figure 1: Performance when detecting moderately-sized (~0.3 mV) smEPSPs as a function of time to the nearest neighbour with realistic mini rates (20, 40, 80 minis/s). Paler shaded colours indicate 95% confidence intervals.

(A) True positive rate (TPR).

(B) False positive rate (FPR).

(C) Sensitivity index d' (undefined but arbitrarily high for TPR > 0 and FPR = 0, e.g. for inter-mini intervals below 1 ms, for minis algorithm).

(D) Cumulative TPR.

(E) Cumulative FPR.

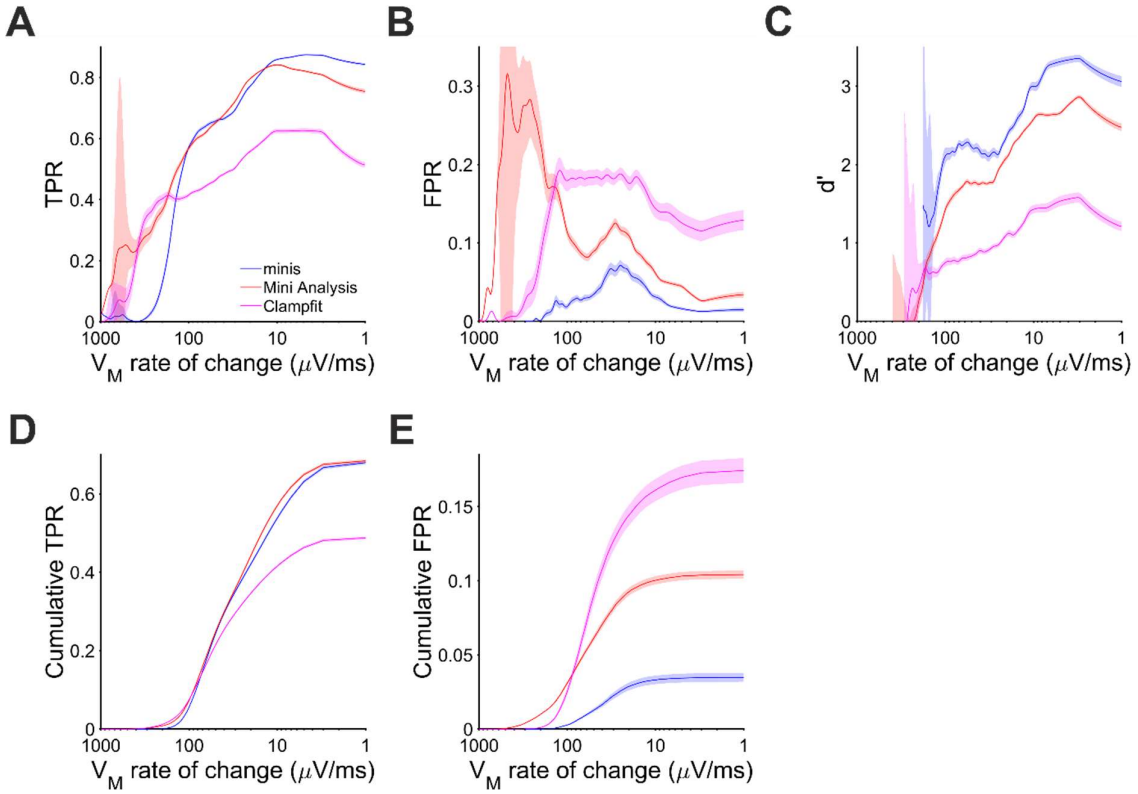

Supplementary Figure 2: Performance when detecting moderately-sized (~0.3 mV) smEPSPs on the rising trend V_m phases with realistic minis' rates (20, 40, 80 minis/s, as in Fig. 9), as a function of the rate of change of V_m. Pale shaded colours indicate 95% confidence intervals.

(A) True positive rate (TPR)

(B) False positive rate (FPR).

(C) Sensitivity index d'.

(D) Cumulative TPR.

(E) Cumulative FPR.

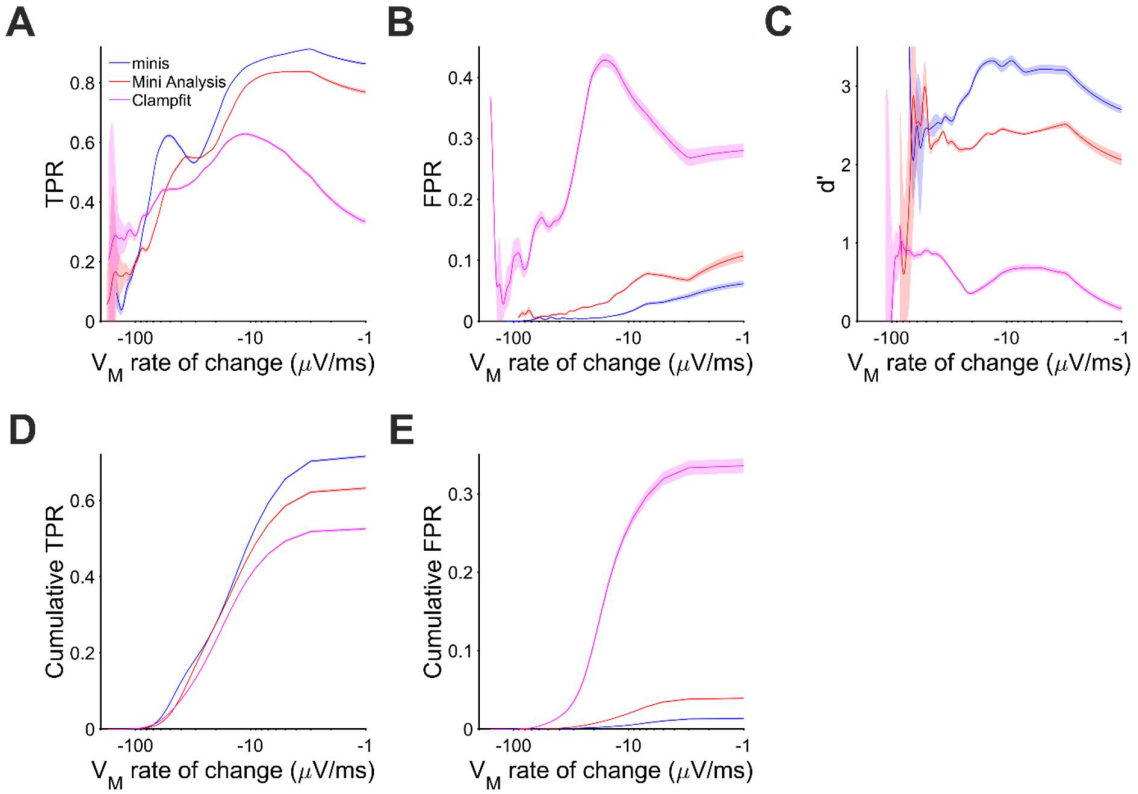

Supplementary Figure 3: Performance when detecting moderately-sized (~0.3 mV) smEPSPs on the membrane potential decay phase with realistic minis rates (20, 40, 80 minis/s, as in Figs. 9 and 10). Pale shaded colours indicate 95% confidence intervals.

(A) True positive rate (TPR) when detecting moderately-sized smEPSPs on the V_m decay phase as a function of the V_m rate of change.

(B) False positive rate (FPR).

(C) Sensitivity index d'.

(D) Cumulative TPR.

(E) Cumulative FPR.